1.0

1.1

1.25 1.4 1.6

4.5
5.0

2.8 2.5
3.2 2.2
3.6
4.0 2.0

1.8

MICROCOPY RESOLUTION TEST CHART

LEVEL

THREE-DIMENSIONAL INTERNAL FLOWS

IN TURBOMACHINERY

VOLUME II

FINAL REPORT

ON

AFOSR CONTRACT F49620-78-C-0041

January 1978 to June 1980

Principal Investigators: K.N. Ghia, and
U. Ghia

REPORT DOCUMENTATION PAGE

	READ INSTRUCTIONS BEFORE COMPLETING FORM

1. REPORT NUMBER	2. GOVT ACCESSION NO.	3. RECIPIENT'S CATALOG NUMBER
AFOSR TR-80 - 1 2 1 5	AD-A093 130	

4. TITLE (and Subtitle)	5. TYPE OF REPORT & PERIOD COVERED
THREE-DIMENSIONAL INTERNAL FLOWS IN TURBOMACHINERY, VOL. II.	FINAL rept. Jan 78 - Jun 80,
	6. PERFORMING ORG. REPORT NUMBER

7. AUTHOR(s)	8. CONTRACT OR GRANT NUMBER(s)
Kirti N. Ghia and Urmila Ghia	F49520-78-C-0041

9. PERFORMING ORGANIZATION NAME AND ADDRESS	10. PROGRAM ELEMENT, PROJECT, TASK AREA & WORK UNIT NUMBERS
Department of Aerospace Engineering & Applied Mechanics, University of Cincinnati, Cincinnati, Ohio 45221	2307/A4 A4 61102F

11. CONTROLLING OFFICE NAME AND ADDRESS	12. REPORT DATE
Air Force Office of Scientific Research/NA Building 410 Bolling Air Force Base, D.C. 20332	Jun 80 70
	13. NUMBER OF PAGES 63

14. MONITORING AGENCY NAME & ADDRESS(if different from Controlling Office)	15. SECURITY CLASS. (of this report)
	Unclassified
	15a. DECLASSIFICATION/DOWNGRADING SCHEDULE

16. DISTRIBUTION STATEMENT (of this Report)

Approved for Public Release; Distribution Unlimited.

17. DISTRIBUTION STATEMENT (of the abstract entered in Block 20, if different from Report)

18. SUPPLEMENTARY NOTES

19. KEY WORDS (Continue on reverse side if necessary and identify by block number)

Three-Dimensional Internal Flows	Elliptic, Semi-Elliptic & Parabolized
Laminar and Turbulent	Navier-Stokes Equations
Incompressible & Compressible	Flow Separation
Circular, Rectangular & Polar	k-ε Turbulence Model
Curved Ducts	Implicit Numerical Methods

20. ABSTRACT (Continue on reverse side if necessary and identify by block number)

Several aspects of viscous internal flows, related to turbomachinery applications, are examined and studied with the use of appropriate model problems. Laminar as well as turbulent flows are considered. In particular, duct flows are studied in detail so as to better understand the physical phenomena occurring therein. This enables their appropriate formulation and, consequently, permits accurate numerical solutions to be obtained efficiently. Configurations involving complex geometry, transverse curvature, longitudinal

410677

DD FORM 1473 EDITION OF 1 NOV 65 IS OBSOLETE

19.

Direct Poisson Solvers
Spline Discretization
Velocity Pressure Formulation

20.

curvature and streamwise flow separation are studied in detail.

Turbulent flows through regular cross-section ducts are studied via the
use of a two-equation model for the turbulence kinetic energy and its dis-
sipation rate. Two approaches for treating the wall regions are examined
and compared. Detailed results are obtained for flow through curved ducts
of polar cross section. Some effort is also made towards modelling anisotropy
and compressibility in turbulent flow using simple model problems.

In the entire study, emphasis is given to the accuracy and efficiency
of the numerical solutions. This has involved the study and implementation
of implicit and semi-implicit numerical schemes of higher-order accuracy and
higher efficiency.

ABSTRACT

Several aspects of viscous internal flows, related to turbomachinery applications, are examined and studied with the use of appropriate model problems. Laminar as well as turbulent flows are considered. In particular, duct flows are studied in detail so as to better understand the physical phenomena occurring therein. This enables their appropriate formulation and, consequently, permits accurate numerical solutions to be obtained efficiently. Configurations involving complex geometry, transverse curvature, longitudinal curvature and streamwise-flow separation are studied in detail.

Turbulent flows through regular cross-section ducts are studied via the use of a two-equation model for the turbulence kinetic energy and its dissipation rate. Two approaches for treating the wall regions are examined and compared. Detailed results are obtained for flow through curved ducts of polar cross section. Some effort is also made towards modelling anisotropy and compressibility in turbulent flow using simple model problems.

In the entire study, emphasis is given to the accuracy and efficiency of the numerical solutions. This has involved the study and implementation of implicit and semi-implicit numerical schemes of higher-order accuracy and higher efficiency.

TABLE OF CONTENTS

ii

LIST OF FIGURES

SECTION 1

INTRODUCTION

In order to better understand complex three dimensional internal flows in turbomachinery, a two-year research project was undertaken. Both laminar and turbulent flow analysis were undertaken to achieve the objectives set forth in this project. The fundamental goal of the laminar study was to develop an analysis and numerical technique for the solution of the three-dimensional parabolized Navier-Stokes equations using a system of surface-oriented coordinates suitable for ducts of arbitrary geometry. The secondary objective was to develop a simplified analysis, which does not require the use of the fully elliptic Navier-Stokes equations, to treat streamwise flow separation satisfactorily. The turbulent flow work was undertaken with a view to improve the use of the second-order closure two-equation isotropic turbulence model in the wall region of simple duct flows. An additional objective of the study was to assess the effect of use of an anisotropic turbulence model for an appropriate flow field.

The follwing five problems have been studied in order to contribute meaningfully towards the goals laid out in this project.

    i.   Laminar flow through ducts of arbitrary cross sections - Joukowski ducts.

    ii. Laminar flow through curved polar ducts.

1

iii. Laminar streamwise separation using a model problem - the Conformal Channel.

iv. Turbulent flow through ducts of simple cross sections, including polar cross section.

v. Effect of anisotropic turbulence modelling and compressibility on turbulent flows.

During the course of the work on each of these problems, emphasis is placed on the accuracy and efficiency of the numerical solutions. For meaningfully achieving this purpose, the following two additional areas of numerical analysis have been carefully studied:

vi. Numerical Analysis:

• Higher-order accuracy of numerical solutions, and

• Development of efficient numerical algorithms.

Suitable model problems have been used, whenever essential, in the research with the overall goal of contributing to the methodology and understanding of internal flows in turbomachinery. Each of the above research areas is described briefly in the following sections and the results and conclusions obtained are summarized.

SECTION 2

LAMINAR FLOW THROUGH DUCTS OF ARBITRARY CROSS SECTIONS -

JOUKOWSKI DUCTS

The study of laminar flow through Joukowski ducts has been completed. This configuration [Fig. 1] provides a model problem containing some of the essential complexities encountered in turbomachinery blade passages. The three-dimensional viscous flow through a duct containing Joukowski airfoil profiles on two of its opposite walls was analyzed and computed using numerically generated surface-oriented coordinates. The computational details of this study were presented in a technical paper (Ref. 1) at the Second International Conference on Mathematical Modelling in July, 1979, St. Louis, Missouri. The main results of the flow problem itself were presented at the ASME 1979 Winter Annual Meeting in New York, in December 1979; a written version of the paper (Ref. 2) appears in the Symposium Proceedings. This study has provided an important fundamental step towards the analysis of three-dimensional viscous flow in the complex geometries of turbomachinery cascades.

SECTION 3

LAMINAR FLOW THROUGH CURVED POLAR DUCTS

The study of laminar flow through curved ducts of polar cross section [Fig. 2] has been brought to a reasonable level of completeness. In addition to the comprehensive results determined for a wide range of the duct curvature parameter, namely, the Dean number K, solutions have also been obtained for some configurations where the upper wall rotates at constant angular velocity. Clockwise as well as counter-clockwise rotation of the upper wall are considered and correspond, respectively, to negative and positive values of the Reynolds number Re_w characterizing the wall motion.

Figure 3a shows the effect of Re_w on the streamwise development of the centerline axial velocity w_{c_L} for the curved polar duct. The case of $Re_w = 0$ is also included here. As Re_w is increased through +10 to +50, the asymptotic value of w_{c_L} decreases, while the oscillatory approach of w_{c_L} to its asymptotic value increases. This behavior is similar to the effect of increasing Dean number K [Fig. 4]. In fact, a closer examination of the cross flow shows that for K = 100 and $Re_w = 0$, the cross flow near the mid-surface r = 1.5 is directed towards the outer wall $\theta = \theta_1$. Consequently, the cross flow near the walls at r = 1.0 and r = 2.0 is directed towards the inner wall $\theta = \theta_2$, i.e., v > 0 near r = 2.0. Hence, $Re_w > 0$ tends to enhance the cross flow and, therefore, has an effect similar to that of increasing K. Conversely, $Re_w < 0$ has an effect similar to that

4

of reducing K, so that the asymptotic value of w_{C_L} increases as Re_w is decreased through -10 to -50. The corresponding stream-wise variations of the maximum axial velocity w_{max} and the mean viscous pressure p_m are shown in Fig. 3b. The behavior of w_{max} is consistent with that of w_{C_L} in Fig. 3a. For increasing positive values of Re_w, w_{C_L} attained lower asymptotic values; hence, the corresponding w_{max} attains higher asymptotic values as seen in Fig. 3b. For analogous reason, decreasing negative values of Re_w lead to lower asymptotic values for w_{max}. Also, the approach to these asymptotic values of w_{max} is very nearly mono-tonic. The similarity between the effects of Re_w and K is most clearly seen from the streamwise behavior of the mean viscous pressure p_m. As Re_w increases from -50, through -10, 0, $+10$, to $+50$, the mean-viscous pressure drop increases monotonically.

A qualitative but clear pictorial view of the effect of Re_w on the flow velocities is obtained from Figs. 5a and 5b. Figure 5a shows the contours of axial velocity in the fully developed flow for $Re_w = -50$, 0 and $+50$. In all three cases, the maximum value of w occurs near the upper right corner, i.e., near the upper wall [$r = 2.0$] and the outer wall [$\theta = \theta_1$]. The w contours for $Re_w = +50$ are considerably more distorted as compared to the w contours for $Re_w = 0$. The associated increase in w_{max} is also seen from the occurrence of the contour value $w = 1.9$ for $Re_w = +50$. For $Re_w = -50$, the w contours become less distorted than those for $Re_w = 0$. It would be interesting to investigate a quantitative relation between Re_w and K such that, for a given K, an appropriate

5

negative value of Re_w could restore almost complete symmetry in the w-velocity distribution and minimize the drop in the mean viscous pressure p_m.

The effect of Re_w on the cross-flow in the curved polar duct is presented in Fig. 5b which shows the direction and the magnitude of the transverse velocity vectors in the fully developed flow. In these computer-generated plots, the duct cross section is laterally inverted, so that the θ-coordinate increases in the clockwise direction in this figure. Hence, the left boundary corresponds to the outer wall $\theta = \theta_1$ and the right boundary corresponds to the inner wall $\theta = \theta_2$ in Fig. 5b. The cross-flow streamlines can be easily traced from the transverse velocity vectors presented. For $Re_w = 0$, the cross flow corresponds basically to two counter-rotating eddies of nearly equal strength, one occupying approximately the lower half and the other occupying the upper half of the duct cross section. The corresponding v velocity is positive near the upper wall. Since a positive value of Re_w makes an additional positive contribution to this v velocity, the upper eddy grows in strength as well as extent while the lower eddy loses some strength and is forced downward as well as towards the two side walls [$\theta = \theta_1$ and $\theta = \theta_2$]. A negative value of Re_w has the opposite effect, i.e., the lower eddy grows in strength as well as size while the upper eddy diminishes. It is interesting to note, however, that although the lower eddy grows in the radial direction, its tangential extent is somewhat diminished, as some cross flow moves downward along the inner wall [$\theta = \theta_2$]. This

sets up an additional weak and elongated eddy occupying nearly the entire inner wall.

The study provides an analysis and a numerical method of solution for flows in curved polar ducts of significant practical interest. To the best knowledge of the authors, flow through curved polar ducts has not been previously analyzed. Hence, the present study provides the first set of available results for this important configuration. A technical paper (Ref. 3) based on the present analysis and results was presented at the AIAA 12th Fluid and Plasma Dynamics Conference in July, 1979, at Williamsburg, Virginia.

Dean's instability as defined, for curved square ducts, by the appearance of an additional pair of counter-rotating vortices near the outer curved wall, was not observed for curved polar ducts of aspect ratio 2/3 for Dean number as high as 630. A systematic study is presently being performed for the fully developed flow in curved polar ducts, using the appropriate asymptotic equations, to analyze the possibility of this phenomenon for the present configuration. These asymptotic solutions will also provide the only available quantitative check on the accuracy of the fully developed flow generated by the present analysis. Also, two further generalizations of the present configuration can be considered. One relates to the consideration of polar ducts with arbitrarily varying radius of longitudinal curvature [i.e., $R = R(\phi)$] as was done by Rushmore and Taulbee (Ref. 4) for arbitrarily curved pipes. Secondly, rotation of the entire

duct, with the upper wall rotating in the opposite direction, can also be considered. This configuration further approaches the rotating blade passages in turbomachinery applications.

SECTION 4

LAMINAR STREAMWISE SEPARATION USING A MODEL PROBLEM -

THE CONFORMAL CHANNEL

In the preceding Grant year, a semi-elliptic formulation
and solution procedure had been developed for analyzing the
laminar incompressible streamwise-separation problem. This study
has been continued and has now been brought to a fair degree of
completeness. The flow in a channel with an asymmetric wall
distortion is studied. For a specified height of the wall
distortion, as the flow Reynolds number is increased, the flow
encounters a bounded region of separation downstream of the
lower-wall distortion [Fig. 6]. Further increase in the Reynolds
number leads, in addition, to recirculating flow regions upstream
of the lower-wall distortion as well as downstream of the upper-
wall distortion.

The problem is formulated in terms of the flow velocity
and pressure using the parabolized momentum equations. Mass
conservation is enforced via an elliptic pressure equation which
also introduces upstream influence in the flow and serves to make
the flow solution regular at the separation points. Surface-
oriented coordinates are generated using a conformal transformation;
further coordinate transformations are employed in order to provide
desired clustering of the computational grid points in the boundary-
layer regions near the channel walls as well as in the recirculating-
flow regions upstream and downstream of the channel-wall distortions.
For the doubly infinite channel considered, a new bounded pressure

9

variable is defined as the difference in the actual pressure distribution and the pressure distribution for the corresponding flow through a straight channel of infinite length. Special care is taken to maintain uniform second-order accuracy of the finite-difference representation for the normal derivatives, especially at the channel walls. A semi-implicit numerical method of solution is employed and results have been obtained for several configurations of the channel geometry characterized by a parameter a^2 and the minimum channel-width H occurring at the position of maximum constriction. The test value of the Reynolds number Re was taken to be 100. Some results are also obtained for Re = 1000 as an attempt to seek the trends predicted by Smith (Refs. 5, 6). The details of the analysis and results were presented (Ref. 7) at the Symposium on Computers in Aerodynamics in June, 1979, at Farmingdale, New York; a final version of the paper is to appear in the International Journal of Computers and Fluids. A few representative results are included here in this report.

A typical distribution of the transformed coordinates for the channel is shown in Fig. 6. In this figure as well as for the streamline patterns that follow, the upper half of the figure represents a magnification of the region in the vicinity of the constriction in the channel shown in the lower half of the figure. Figure 7 shows the streamline contours in the physical plane for a typical channel configuration for Re = 100. The values of the stream function along the contours are listed in Table I.

The channel with $a^2 = 0.585$ and $H = 0.678$ shows a region of recirculation downstream of the maximum constriction, and extending approximately over the range $0.89 < \zeta < 2.05$. An increase in the severity of the channel constriction seems to have little influence on the position of the separation point, but causes a small downstream shift of the reattachment point. The results bear strong similarities with the experimentally visualized flow patterns given by Lee and Fung (Ref. 8) for flow in pipes with symmetric constrictions for Re = 31, 70 and 185. The eddy in the present configurations is considerably shorter due to the manner in which the upper wall bends towards the lower wall downstream of the constriction. If the upper wall of the channel were a mirror-image of the lower wall, reattachment would clearly occur farther downstream.

The streamline contours presented in Fig. 7 are obtained from the semi-elliptic formulation. The corresponding elliptic solutions are so nearly the same as the semi-elliptic solutions that they would be indistinguishable in terms of streamline patterns. For a more meaningful evaluation of the semi-elliptic formulation, Figs. 8a and 8b present a comparison of the semi-elliptic results and the elliptic results for the shear-stress parameter $\partial w/\partial \eta$ and the pressure variable $\tilde{p}$ at the channel walls.

The shear stress at the lower wall is positive everywhere except between the separation and the reattachment points. On the other hand, the shear stress at the upper wall is negative everywhere except in a recirculation region, if one does occur,

11

near the upper wall. Deviation from zero slope of the curves of $\partial w/\partial \eta$ vs. ζ upstream of the constriction may be viewed as a measure of the upstream influence due to the constriction. In terms of the results for the surface shear [Fig. 8a], the semi-elliptic model yields solutions that are in excellent agreement with the elliptic solutions, although some differences are observed for cases with severe separation. It is presently felt that these differences may be, in part, because the results presented may not be the fully converged solutions of the governing equations. The rather slow convergence rate of the severely separated flow solutions led to terminating the calculations after a prescribed amount of computer time (10 minutes on an Amdahl 470/V6 computer). Hence, the solutions obtained may be at different levels of convergence. It is believed that, with further iterations, the results would remain qualitatively unchanged. Nevertheless, it appears safe to state that, in all cases, the separation encountered is regular and the semi-elliptic formulation is free from the separation singularity.

Figure 8b shows the behavior of the corresponding surface pressure in terms of the quantity $\tilde{p}$ which represents the deviation in the channel pressure due to the effects of the constriction. Again, the semi-elliptic results agree well with the elliptic results, (except for cases with severe separation, for reasons mentioned in the preceding paragraph). The more important point to be observed from these surface-pressure results is the extended region of upstream influence of the constriction on the surface.

This also indicates the appropriateness of retaining ellipticity in the pressure equation. It should also be observed that the downstream value of $\tilde{p}$ represents a measure of the additional pressure loss occurring as a result of the constriction in the channel. This is seen to increase with increasing severity of the constriction and the separation.

A general observation to be made from the solution obtained is that the semi-elliptic model developed in the present study is regular at separation. Since the dependent variables used in the formulation are the velocities and the pressure, the formulation should be directly extendable for three-dimensional flows. Of particular interest are some curved-duct configurations as those encountered in turbomachinery cascades.

The results obtained from the semi-elliptic formulation and their comparison with the corresponding Navier-Stokes solutions are very encouraging. Also, the general agreement of some of the qualitative flow features observed in the results for Re = 1000 with those predicted by the asymptotic analysis of Ref. 6 indicates that the present formulation should be investigated further.

For instance, it would be worthwhile to consider constrictions that are longitudinally more confined than the present ones, in order to determine, more quantitatively, the position of the upstream separation point with respect to the starting point of the constriction. Also, the relative magnitude of the elliptic terms in the momentum equations should be assessed in order to justify neglecting them. The use of upwind differencing for the

streamwise convective terms should be evaluated with respect to its influence on the accuracy and the convergence of the solutions. As observed earlier (Ref. 9), upwind differencing generally accelerates the convergence rate while reducing the order of accuracy of the results. The resolution of the present solutions needs further improvement for higher Re cases. This may be achieved by the combined use of a finer grid in the critical regions and a higher-order accurate solution procedure such as the fourth-order accurate solution procedure such as the fourth-order accurate simplified spline procedure of Rubin and Khosla (Ref. 10). The discretized representation of the pressure equation must be consistent with the discretized representation of the velocity divergence in order to minimize errors in satisfying the local continuity equation. The present solution procedure also needs to be examined further in order to achieve better convergence rates. Several of these factors are presently under further investigation.

SECTION 5

TURBULENT FLOW THROUGH DUCTS OF SIMPLE CROSS SECTIONS,
INCLUDING THE POLAR CROSS SECTION

The turbulent flow in curved ducts of simple cross sections
was studied further. The turbulent stresses were modelled via
an equivalent isotropic eddy viscosity determined from the
turbulent kinetic energy k and its dissipation rate ε. The
two-equation model of Launder and Spalding (Ref. 11) was suitably
modified to provide k and ε. In the wall regions, the deter-
mination of k and ε invokes either the law of wall or the low
Reynolds-number modelling (LRM) approach of Jones and
Launder (Ref. 12). The wall-function (WF) method has the
disadvantage that boundary conditions are not imposed very
rigorously at the walls. On the other hand, if the boundary
conditions are satisfied at the duct wall, the various layers
of the 'inner region' including the region where the laminar
viscosity also has a significant influence, must be resolved
satisfactorily. The number of grid points necessary for the
required resolution results in large computation grids and,
hence, leads to excessive computing times. This problem of large
grids was resolved by the use of suitable analytical transfor-
mations for the cross-plane coordinates in order to provide
reasonable resolution of the high-gradient regions near the
duct walls. The two methods for the wall regions were evaluated
by computing the flow in a curved circular pipe and comparing
the resulting solutions with available data for curved circular

15

pipes. Detailed solutions were obtained for the turbulent flow in curved polar ducts for various values of the problem parameters (see Ref. 13). Typical results for some of these configurations are described in the present report.

5.1 Curved Circular Pipe with $Re_D = 25,000$, R = 20

For this case, both experimental data as well as analytical predictions are available in the literature. Moreover, this case has an additional significance, namely, that the wall region can be treated by both the WF method as well as the LRM approach. For the wall-function method, the boundary conditions were applied at $y_+ = 35$, whereas, for the low-Reynolds number modelling approach, the first node was located at $y_+ = 3.1$, well within the viscous sublayer. The fully developed profiles of the normalized axial velocity w/w_{cl} at sections AA and BB, shown in the inset of Fig. 9, are compared with the experimental data of Mori and Nakayama (Ref. 14) and the theoretical predictions of Patankar, Pratap and Spalding (Ref. 15) in Fig. 9. Because of the symmetry of the flow across section AA, the axial velocity profile along section BB is plotted for only half the pipe diameter along BB. Present predictions obtained using the WF method agree well with the data of Ref. 14 as well as with the predictions of Ref. 15 where also the wall-region was treated using wall functions. On the other hand, the LRM approach leads to results that agree best with the experimental data shown, as seen especially from the profile along section AA. In a narrow region near the outer wall, none of the computed results shown

16

in this figure are able to predict the experimentally observed large velocity-gradients created by the large centrifugal forces in this region. In general, it may be stated that the turbulence closure model used predicts the fully developed mean-flow axial velocity profiles satisfactorily. The LRM approach is found to be slightly superior to the wall-function method. Also shown in this figure are the results of Sokhey et al. (Ref. 16) using the WF method with a (41 x 11) uniform grid. The present results of the WF method are obtained using a (21 x 11) non-uniform grid, and are seen to almost reproduce the (41 x 11) uniform-grid solutions of Sokhey et al. (Ref. 16). This latter comparison serves to further establish the usefulness of the cross-plane coordinate transformation employed in the present work.

5.2 Comparative Study of Wall-Region Treatment by WF Method and LRM Method

The three flow configurations considered for this comparative study are the following:

   i.   Curved Circular Pipe with $Re_D = 25,000$, $R = 20$;

   ii. Curved Polar Duct with $Re_D = 25,000$, $R = 20$, $AR = 1.0$;

   iii. Curved Square Duct with $Re_D = 25,000$, $R = 20$.

The results of this comparative study have been examined in light of the advantages and disadvantages these two methods have. To summarize, the WF method is applicable for moderate to high Reynolds numbers but has the disadvantage that the boundary conditions are not satisfied exactly at the walls. Also, the present form of the law of the wall used does not account for

17

the effects of curvature. On the other hand, the LRM method
satisfies the wall-boundary conditions more accurately, but has
the disadvantages of being limited to flows with moderate
Reynolds number and requiring larger computational grids.

5.2.1 Curved Circular Pipe with Re_D = 25,000, R = 20

The mean-flow as well as turbulence quantities are examined
in detail in this comparative study. The streamwise variation
of the centerline axial velocity w_{C_L} and the drop in mean
pressure p_m are presented in Fig. 10 for the curved circular
pipe with Re = 25,000 and R = 20. Compared to the LRM method,
the WF method is seen to under-predict the maximum value as
well as the asymptotic value of w_{C_L} by 3 percent and 1 percent,
respectively. Consequently, the corresponding mean-pressure
drop predicted by the WF method is somewhat smaller than that
predicted by the LRM method. The oscillatory streamwise
development of the centerline velocity had been observed earlier
for the corresponding laminar flow also; it is a characteristic
of curved-duct flows. For turbulent flow, Patankar, Pratap
and Spalding (Ref. 15) have also reported similar oscillations
in the centerline velocity. The streamwise development of axial
velocity profiles along the planes BB and AA is presented in
Fig. 11. The mean-flow axial velocity profiles are not
significantly affected by differences in the method of treating
the wall region. The developing secondary-flow profiles of
u-velocity at three different r-locations in the cross plane
and three different streamwise positions are presented in Fig. 12a.

18

For curved ducts, non-zero secondary-flow velocities exist even in the fully developed state. If the results of the LRM method are taken as a norm, the WF method shows smaller magnitudes of u-velocity near the inside ($r = 1$, $\theta = \pi$) as well as near the outside ($r = 1$, $\theta = 0$) of the bend. The v-velocity profiles at two different θ-locations are presented in Fig. 12b at the same three streamwise positions. Near the outer wall, there is significant v-velocity and, again, the peak values predicted by the LRM method are of larger magnitudes than those obtained by the WF method. The corresponding fully developed profiles of u- and v-velocities are presented in Fig. 12c. This figure shows that, only for $(\theta-\theta_1)/(\theta_2-\theta_1) = 0.2$, both the wall-region methods used yield identical r-profiles of v-velocity; for all other profiles, the LRM method yields larger values for the peaks as compared to the results obtained by the WF method.

5.2.2 <u>Curved Polar Duct and Curved Square Duct With</u>

   <u>$Re_D = 25,000$, $R = 20$, $AR = 1.0$</u>

The flow in curved rectangular ducts exhibits symmetry only across plane AA. But even this symmetry is lost for the flow in curved ducts with polar cross section. The turbulent flow results obtained by the WF method and the LRM method for ducts of rectangular and polar cross section are compared here.

Figure 13 shows the streamwise development of the centerline velocity $w_{\mathbb{C}_L}$. The streamwise oscillatory behavior of $w_{\mathbb{C}_L}$ is again clearly seen here. For both configurations, the peaks predicted by the LRM method are more pronounced than, and occur

19

slightly upstream of, the peaks predicted by the WF method.

Although the results obtained by the WF method for both these

duct configurations are about the same, the results using the

LRM method show a maximum difference of about 5 percent

between w_{C_L} for the polar and the square duct configurations.

Also shown in this figure are the streamwise variations of the

mean-pressure drop for both these duct configurations and,

again, the LRM method leads to a much larger pressure drop than

that predicted by the WF method. The developing secondary u-

and v-velocity profiles are depicted in Figs. 14a and 14b,

respectively. These figures do not show the corresponding results

for the duct of square cross section since such a comparison is

not meaningful for the cross-flow velocities because of the

differences in the direction of Cartesian and polar components

of velocity. Only in one orientation, namely, for $\theta = \pi/2$,

such a comparison could lead to some useful information. The

corresponding fully developed secondary u- and v-velocity

profiles are shown in Fig. 14c. It appears that the predictions

obtained by both the wall-region methods are about the same.

The findings of the comparative study of the two wall-

region methods indicate that, for the curved circular pipe, the

turbulence closure problem has been treated appropriately and

that the LRM method leads to slightly better predictions than

the WF method, since it treats the wall region more accurately.

However, the results presented for the curved ducts of

rectangular and polar cross sections show significant deviations

even in the mean-flow variables predicted by the two wall-

20

region methods. This still does not answer the question, namely, which of the two models is more suitable for duct-flow analyses. Additional experimental data for the curved duct of rectangular cross section can serve to alleviate this problem that is faced presently.

5.3 Parametric Study for Curved Polar Ducts

For the curved polar-duct configurations, some of the parameters of interest are the aspect ratio AR of the duct cross section and the radius R of longitudinal curvature of the duct. The effect of variation of these parameters on the resulting flow field is examined in this section. Three different aspect ratios, namely, AR equal to 2/3, 1 and 3/2, and three values of the radius of curvature, namely, R equal to 10, 20 and 50, are considered. The Reynolds number based on hydraulic diameter is maintained at 50,000. Only the wall function method is used to treat the wall region, as the LRM method developed still requires a rather large number of grid points for this value of the Reynolds number.

5.3.1 Effect of Aspect Ratio AR

In Fig. 15, the streamwise variations of the centerline axial velocity $w_{\mathfrak{c}}$ and the drop in mean pressure p_m are presented for three different aspect ratios. The aspect ratio was varied in such a manner that the radial dimension (AA in Fig. 2) was held fixed while the tangential dimension (BB in Fig. 2) was appropriately changed. The radius of curvature R is held at 10 for the three configurations examined. The inlet velocity was

21

appropriately adjusted to maintain the same entrance mass flow for all three configurations. The centerline velocity w_{q_L} shows streamwise oscillations similar to those observed earlier for other curved-duct configurations. The peak value of w_{q_L} increases with increase in aspect ratio. For all three cases, the centerline velocity asymptotes to the fully developed centerline value by $z \simeq 50$. The streamwise variation of the mean-pressure drop is also depicted in this figure but it is seen to be rather insensitive to changes in aspect ratio.

5.3.2 Effect of Variation of Radius of Curvature R

For the curved polar duct of aspect ratio AR = 3/2 and Reynolds number Re = 50,000, the radius of curvature R was varied and its effect on the flow field was examined. The three values considered for the radius of curvature R are 10, 20 and 50. Varying the radius of curvature R, while keeping the Reynolds number Re fixed, is equivalent to changing the corresponding Dean number K. Since $K = Re/\sqrt{R}$, an increase of the radius of curvature leads to a decrease in the value of K.

Figure 16 enables examination of the effect of R on the streamwise variation of the centerline axial velocity w_{q_L} and the drop in mean pressure p_m. The centerline w_{q_L} increases with increase in R, and asymptotes to a larger fully developed value. This behavior is similar to that observed earlier for laminar flow where the corresponding Dean number was decreased. The mean-pressure drop is, again, rather insensitive to the variation in R. The fully developed secondary-flow velocities

22

u and v are depicted in Fig. 17; the profiles of u and v are rather insensitive to the variation in R.

The parametric study carried out in the present research for turbulent flow in curved polar ducts reveals useful qualitative and quantitative information that is not very intuitive. However, further numerical experiments must be conducted in order to more firmly establish the trends observed here in this study.

SECTION 6

EFFECTS OF ANISOTROPIC TURBULENCE MODELLING AND

COMPRESSIBILITY USING MODEL FLOW PROBLEMS

6.1 Asymptotic Compressible Turbulent Corner Flow

This study is carried out with the objective of analyzing turbulent axial-corner flow and, more importantly, for studying the effects of compressibility and turbulence on shock-free asymptotic corner flow in the presence of viscous interactions, namely, the lateral displacement thickness interactions. The turbulence is modelled using the familiar two-layer eddy viscosity model of the form used by Cebeci (Ref. 17) and also with a modified form of the Gessner-Emery anisotropic turbulence model (Ref. 18). Numerical solutions are obtained for a range of Mach numbers and wall-temperature boundary conditions. For some supersonic cases, the effect of suction or injection at the walls is also studied.

The axial 90°-corner flow geometry is depicted in Fig. 18. The asymptotic set of equations governing the flow at the far-field boundary were solved using the numerical method developed in this study. No special treatment is provided for the leading-edge singularity; hence, the results in the very close proximity of the leading edge of the corner geometry must be used with caution. The laminar self-similar results were recovered as the solution progressed in the downstream direction. Gradual transition was then initiated to approach the turbulent flow.

To assess the analysis and the corresponding computer program, results were first obtained for the corresponding adiabatic incompressible flow. This configuration was chosen because Shafir and Rubin (Ref. 19) have studied this configuration and provided numerical results for it. The results of this comparative study are shown by curves 1 and 3 in Fig. 19. A maximum deviation of 10 percent is observed with the present analysis showing higher skin-friction values than those in Ref. 19. This discrepancy led to a further comparative study of a still degenerate case, namely, the flow past a flat plate. For this latter case, experimental data of Weighardt (Ref. 20) are available and so also is the corresponding analytical result given in Ref. 21. Both of these results are also depicted in Fig. 19. To complete this comparison, it was essential to obtain results of the present computations without cross flow. As seen in Fig. 19, the present analysis agrees very favorably with these data. A close examination of the set of governing equations and, in particular, the streamwise momentum equation, reveals that the streamwise component of velocity even at infinity is coupled with the cross-flow equations through the turbulent eddy viscosity ε_{ij} which depends on the normal gradient of the cross-flow velocity w_y. Thus, it is felt that a higher skin-friction coefficient is possible for this quasi-three-dimensional asymptotic flow.

Further, to rule out the possibility that the deviation of the present results from those of Shafir and Rubin (Ref. 19)

could be due to differences in the step sizes in the normal
direction used in these two studies, a step-size study was
conducted for the same configuration. The present calculations
were repeated using a grid identically the same as that used
in Ref. 19, namely, 140 grid points in the normal direction.
The results of this study are presented in Fig. 20 for the stream-
wise velocity u, and the cross-flow velocity w. These show a
maximum deviation of about five percent in the cross flow
velocity component in the laminar flow region, further verifying
the accuracy of the results obtained in the present study with
only 51 grid points in the normal direction. Thus, to conclude,
it is believed that the deviation in the results should be due
to the following factors. Shafir and Rubin (Ref. 19) used a
first-order accurate marching scheme. In the transition region,
the streamwise step size is twice as large in their study and,
further, in the turbulent region that follows, their step-size
is twenty times larger than that used in the present study.
Finally, due to the non-uniform grid, second-order accuracy in
the normal direction is also not possible in their study.

The results for this incompressible configuration were
also studied using the modified form of the anisotropic turbulence
model of Gessner and Emery (Ref. 18). The skin-friction
coefficients obtained using the two different turbulence models
are presented in Fig. 21. The conformity between these two
sets of results led to the conclusion that the effect of
anisotropy is not significant in the study of the asymptotic

corner flow. It also further justifies the use of the simple
two-layer algebraic turbulence model for this study.

A technical paper based on these results is planned for
preparation and will be offered for presentation at the Inter-
national Gas Turbine Conference in Houston, Texas, in
March, 1981. This paper will include detailed results on the
effect of compressibility, turbulence and mass transfer on
the developing flow along an axial corner.

6.2 Three-Dimensional Free-Shear Flow

In order to study the effect of compressibility in the
presence of turbulence, the turbulent free-shear flow exhausting
from a three-dimensional rectangular nozzle [Fig. 22] is
analyzed. The problem is formulated using the time-averaged
Navier-Stokes equations parabolized in the streamwise direction.
Turbulence closure is achieved by a modified form of the
existing two-equation model for turbulence kinetic energy and
dissipation-rate function. Analytical coordinate transformations
are used in the cross-plane to impose the freestream boundary
conditions at true infinity in the two cross-plane directions.
An implicit numerical method is used to obtain the numerical
solutions. For incompressible turbulent flow, solutions have
been obtained for several configurations and compare satisfactorily
with the available data. For compressible shock-free shear flow
also, solutions have been obtained for several flow configurations
and the results are verified with the limited amount of data

27

available. For large aspect ratio ($\alpha \geq 10$), the centerline characteristics of streamwise velocity and temperature are observed to remain invariant.

Two papers were prepared on the basis of this study. The details of the numerical method were presented in a technical paper (Ref. 22) at the Second International Conference on Mathematical Modelling in July, 1979, at St. Louis, Missouri. The significant results of the flow problem were presented (Ref. 23) at the 2nd International Symposium on Turbulent Shear Flows, London, England, in July, 1979.

SECTION 7

NUMERICAL ANALYSIS

7.1 Higher-Order Accuracy of Numerical Solutions

For the purpose of obtaining higher-order accuracy, a
spline formulation is developed for the velocity-pressure form
of the Navier-Stokes equations for incompressible flow. The
equation required for pressure is formulated directly from the
discretized form of the momentum equations using the various
spline relations, so that it is consistent with the discretized
definition of velocity divergence. The analysis is demonstrated
by results computed for the model problem of driven flow in a
cavity. The singularities in this problem are found to enter
the velocity-pressure formulation in an essential manner.
Hence, particular attention is given to the influence of these
singularities by employing an asymptotic analysis to determine
the local Stokes solution at the singular corners and extract
this from the formulation. A modified cavity configuration that
is free of singularities is also considered. The details of
the analysis and the numerical results were presented in a
technical paper (Ref. 24) at the 4th AIAA Computational Fluid
Dynamics Conference in July, 1979, at Williamsburg, Virginia.

7.2 Development of Efficient Numerical Algorithms

Accurate and highly efficient implicit numerical techniques
have been developed for the solution of the two-dimensional
unsteady incompressible Navier-Stokes equations in the derived

29

variables (ω,ψ) as well as in the primitive variables (u,v,p). In addition to the transport equations, the primitive-variable (u,v,p) formulation and the derived-variable (ω,ψ) formulation of the Navier-Stokes equations contain an elliptic Poisson problem with Neumann and Dirichlet boundary conditions, respectively. A significant increase in the computational efficiency of Navier-Stokes solvers has been achieved by employing the direct Poisson solvers of Hockney (Ref. 25) and Bunemann (Ref. 26) for these Poisson problems. A detailed numerical investigation has been carried out for the model problem of a shear-driven two-dimensional square cavity. The present (ω,ψ) results are in excellent agreement with those of previous investigators but are obtained with significant savings in computing time. For the first time, an implicit technique has been developed for solving the Navier-Stokes equations in primitive variables while also providing an arbitrarily small steady-state dilation field. The results of the numerical experimentation conducted were presented in a technical paper (Ref. 27) at the Second International Conference on Mathematical Modelling in July, 1979, St. Louis, Missouri.

SECTION 8

REFERENCES

Note: Superscript asterisk (*) denotes that the work was performed partially or wholly, under AFOSR sponsorship.

1.* Sathyanarayana, K. and Ghia, U., "Numerical Simulation of Three-Dimensional Viscous Flow in Ducts of Arbitrarily Varying Cross Sections," presented at Second International Conference on Mathematical Modelling, St. Louis, Missouri, July 1979.

2.* Ghia, U. and Sathyanarayana, K., "Analysis and Solution of Three-Dimensional Viscous Flow in Non-Rotating Ducts," presented at ASME Winter Annual Meeting, New York, December 1979; appears in Flow in Primary, Non-Rotating Passages in Turbomachines, ASME Publication, Editors: H.J. Herring, A. Soler, and W.G. Steltz, 1979.

3.* Ghia, U., Ghia, K.N. and Goyal, R.K., "Three-Dimensional Viscous Incompressible Flow in Curved Polar Ducts," AIAA Paper 79-1536, presented at AIAA 12th Fluid and Plasma Dynamics Conference, Williamsburg, Virginia, July 1979.

4. Rushmore, W.L. and Taulbee, D.B., "Numerical Investigation of Developing Pipe Flows of Arbitrary Curvature," Computers and Fluids, Vol. 6, 1978, pp. 125-140.

5. Smith, F.T., "Flow Through Constricted or Dilated Pipes and Channels," Parts 1 and 2, Quarterly J. Mech. and Appl. Math., Vol. 29, Pt. 3, 1976, pp. 343-376.

6. Smith, F.T., "Upstream Interactions in Channel Flows," Journal of Fluid Mechanics, Vol. 79, Part 4, 1977, pp. 631-655.

7.* Ghia, U., Ghia, K.N., Rubin, S.G. and Khosla, P.K., "Study of Incompressible Flow Separation Using Primitive Variables," presented at Symposium on Computers in Aerodynamics, Polytechnic Institute of New York, New York, June 1979; to appear in Computers and Fluids, 1980.

8. Lee, J.S. and Fung, Y.C., "Flow in Non-Uniform Small Blood Vessels," Microvascular Research, Vol. 3, 1971, pp. 272-287.

9. Ghia, U. and Davis, R.T., "Navier-Stokes Solutions for Flow Past a Class of Two-Dimensional Semi-Infinite Bodies," AIAA Journal, Vol. 12, No. 12, Dec. 1974, pp. 1659-1665.

10. Rubin, S.G. and Khosla, P.K., "A Simplified Spline Solution Procedure," Proc. Sixth Int. Conf. on Numerical Methods in Fluid Dynamics, Georgian SSR, June 1978.

11. Launder, B.E. and Spalding, D.B., "Numerical Computation of Turbulent Flows," Computer Methods in Applied Mechanics and Engineering, Vol. 3, 1974, pp. 269-289.

12. Jones, W.P. and Launder, B.E., "The Prediction of Laminar-ization with a Two-Equation Model of Turbulence," International Journal of Heat and Mass Transfer, Vol. 15, 1972, pp. 301-314.

13.* Goyal, R.K., Ghia, U. and Ghia, K.N., "Study of Viscous Flow in Ducts Using Parabolized Navier-Stokes Equations," Report No. AFL 80-5-53, Department of Aerospace Engineering and Applied Mechanics, University of Cincinnati, 1980.

14. Mori, Y. and Nakayama, W., "Study on Forced Convective Heat Transfer in Curved Pipes," International Journal of Heat and Mass Transfer, Vol. 10, 1967, pg. 37.

15. Patankar, S.V., Pratap, V.S. and Spalding, D.B., "Prediction of Turbulent Flow in Curved Pipes," Journal of Fluid Mechanics, Vol. 67, 1975, pg. 583.

16.* Sokhey, J.S., Ghia, K.N. and Ghia, U., "Study of Turbulent Flow in Curved Ducts Using a Two-Equation Turbulence Model," Proceedings of First International Conference on Mathe-matical Modelling, St. Louis, Missouri, September 1977.

17. Cebeci, T., "Calculation of Three-Dimensional Boundary Layers: II. Three-Dimensional Flows in Cartesian Coordinates," AIAA Journal, Vol. 13, No. 8, August 1976, pp. 1056-1064.

18. Gessner, F.B. and Emery, A.F., "A Reynolds Stress Model for Turbulent Corner Flows - Part I: Development of the Model," Journal of Fluids Engineering, Trans. ASME, Vol. 98, No. 2, June 1976, pp. 261-268.

19. Shafir, M. and Rubin, S.G., "The Turbulent Boundary Layer Near A Corner," Journal of Applied Mechanics, Trans. ASME, Vol. 43, No. 4, December 1976, pp. 567-570.

20. Wieghardt, K., "Proceedings - Computation of Turbulent Boundary Layers - 1968," AFOSR IFP-Stanford Conference, Editors: D.E. Coles and E.A. Hirst.

21. Cebeci, T. and Smith, A.M.O., "Analysis of Turbulent Boundary Layers," Academic Press, 1974.

22.* Bobba, C.R. and Ghia, K.N., "A Mathematical Model and Numerical Solution of Turbulent Shear Flow," presented at the Second International Conference on Mathematical Modelling, St. Louis, Missouri, July 1979.

23.[*] Bobba, C.R. and Ghia, K.N., "A Study of Three-Dimensional Compressible Turbulent Jets," presented at Second International Symposium on Turbulent Shear Flows, London, England, July 1979; published in Conference Proceedings, pp. 1.26-1.31.

24.[*] Ghia, K.N., Shin, C.T. and Ghia, U., "Use of Spline Approximations for Higher-Order Accurate Solutions of Navier-Stokes Equations in Primitive Variables," AIAA Paper 79-1467, presented at AIAA 4th Computational Fluid Dynamics Conference, Williamsburg, Virginia, July 1979.

25. Hockney, R.W., "The Potential Calculation and Some Applications," Methods in Computational Physics, Vol. 9, Academic Press, New York and London, 1969, pp. 136-311.

26. Buneman, O., "A Compact Non-Iterative Poisson Solver," SUIPR Report No. 294, 1969.

27.[*] Osswald, G.A. and Ghia, K.N., "Use of Direct Poisson Solvers in the Numerical Solution of Navier-Stokes Equations," presented at Second International Conference on Mathematical Modelling, St. Louis, Missouri, July 1979.

TABLE I

VALUES FOR STREAMLINE CONTOURS IN

FIGURE 7

CONTOUR NO.	VALUE OF ψ
1	1.001
2	0.9
3	0.8
4	0.7
5	0.6
6	0.5
7	0.3
8	0.1
9	0.1×10^{-8}
10	-0.001
11	-0.003
12	-0.010
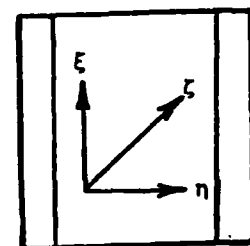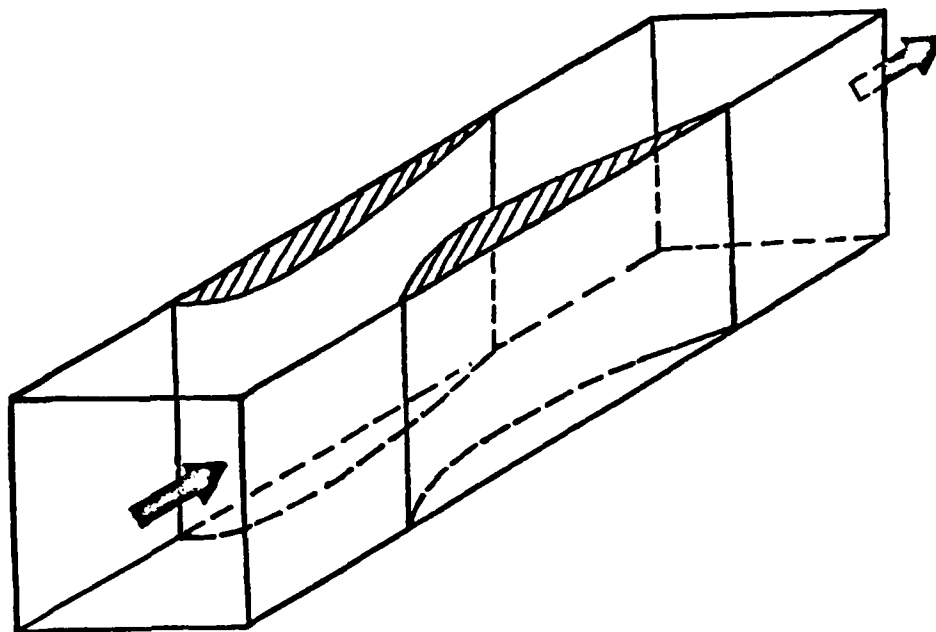
a.   RECTANGULAR JOUKOWSKI DUCT
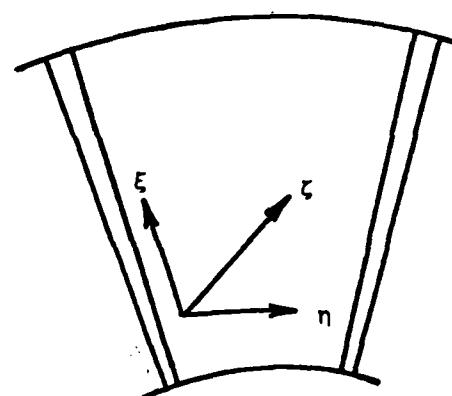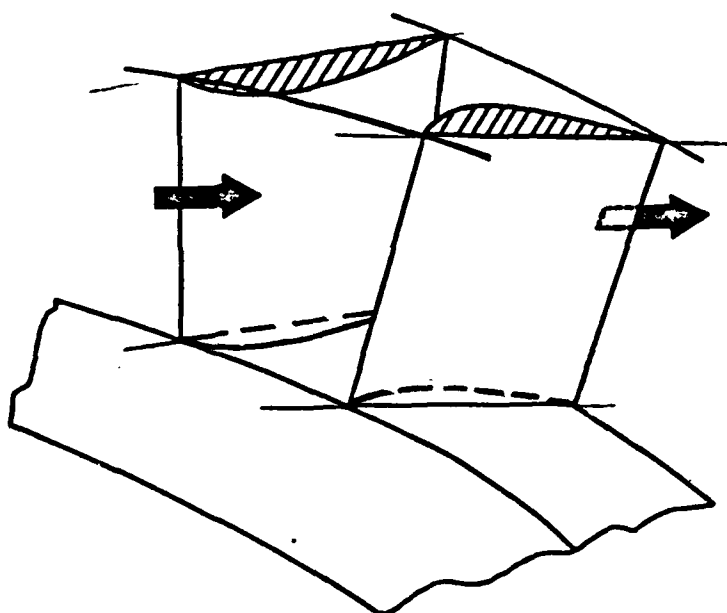
AXIAL VIEW

b.   POLAR JOUKOWSKI DUCT

AXIAL VIEW

FIGURE 1.   SCHEMATIC REPRESENTATION OF SIMPLIFIED CASCADE CHANNELS.

HYDRAULIC DIAMETER
(RECTANGULAR CROSS SECTION)

$$D = 2\ ab/(a+b)$$

HYDRAULIC DIAMETER (POLAR CROSS SECTION)

$$D = \frac{(r_2^2-1)(\theta_2-\theta_1)}{(r_2-1) + \frac{1}{2}(\theta_2-\theta_1)(r_2+1)}$$

REYNOLDS NUMBER

$$Re_D = \frac{w_{in} \cdot D}{\nu}$$

DEAN NUMBER

$$K = Re_D \cdot (1/R)^{1/2}$$
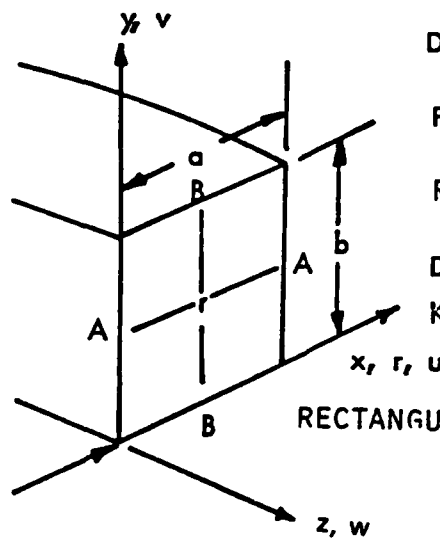
RECTANGULAR CROSS SECTION
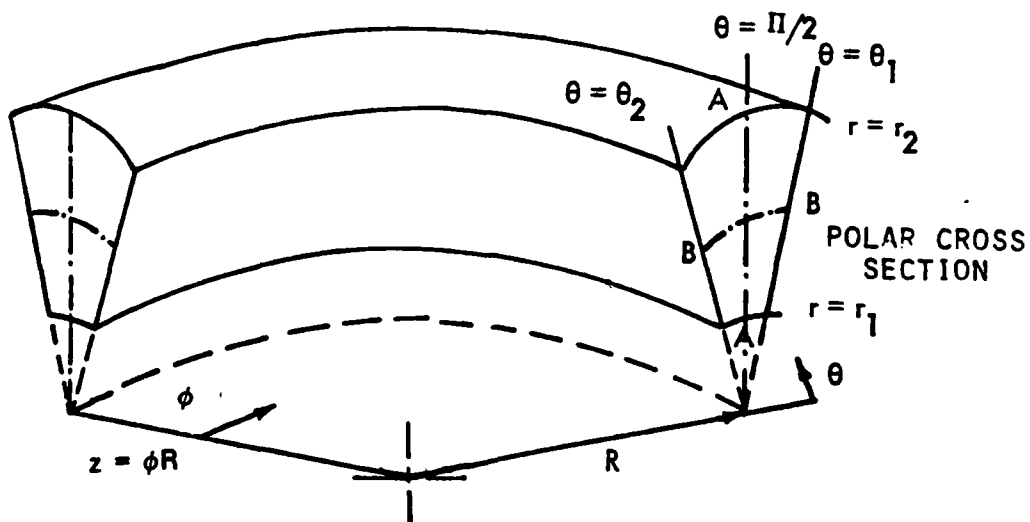
POLAR CROSS SECTION

FIGURE 2. CURVED DUCT GEOMETRY AND COORDINATE SYSTEM

36
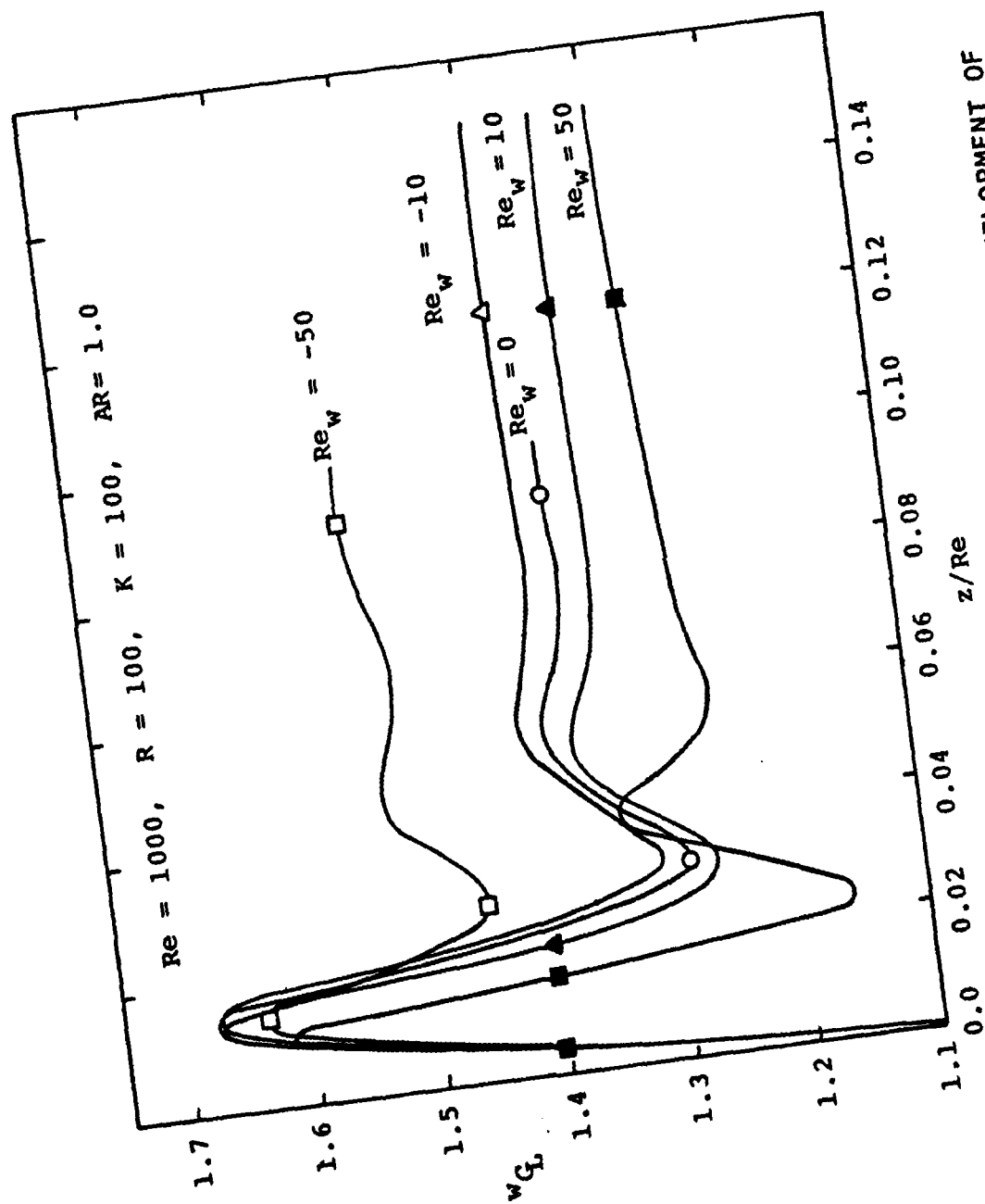
FIG. 3a. EFFECT OF WALL ROTATION ON STREAMWISE DEVELOPMENT OF CENTERLINE AXIAL VELOCITY.
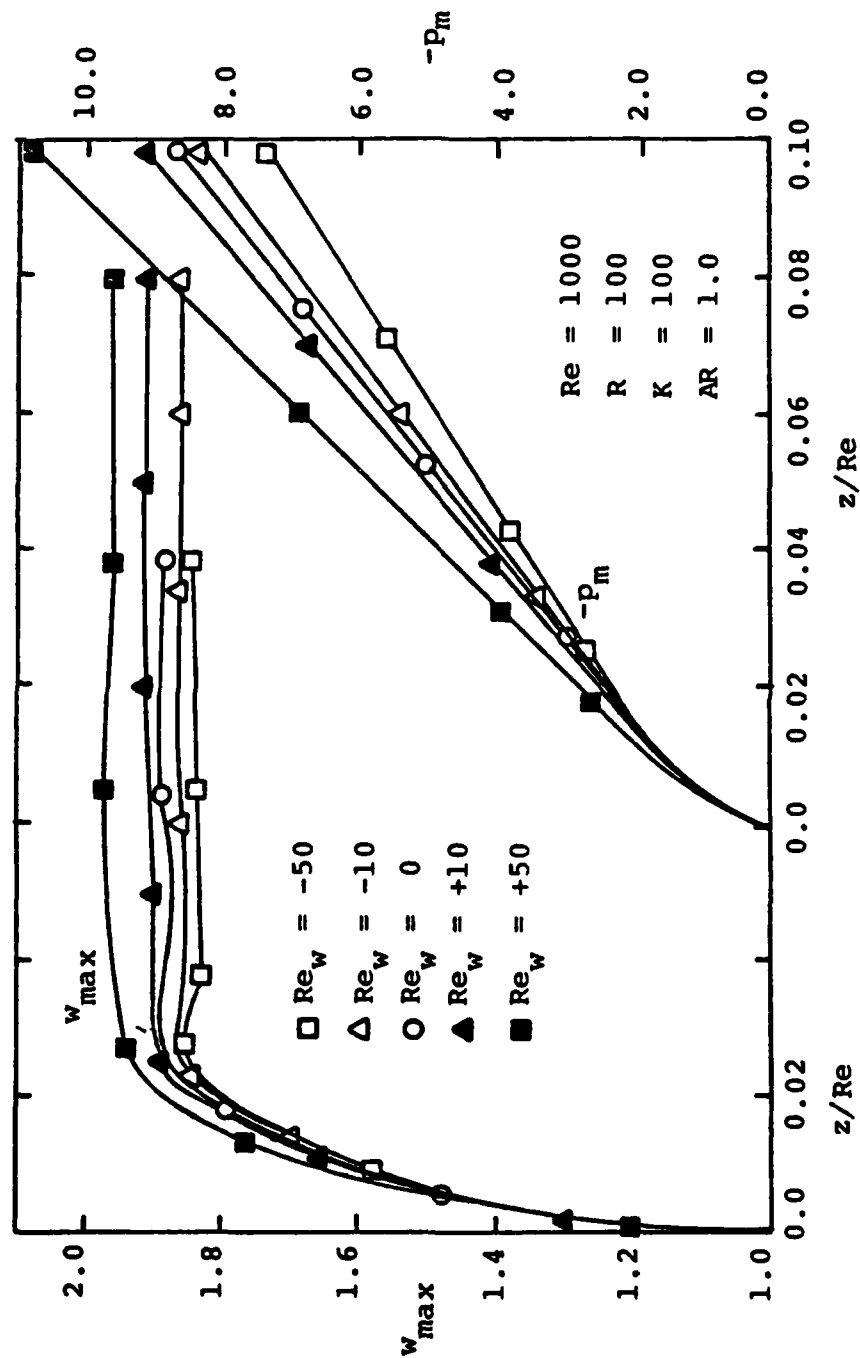
FIG. 3b. EFFECT OF WALL ROTATION ON STREAMWISE VARIATION OF MAXIMUM AXIAL VELOCITY AND MEAN VISCOUS PRESSURE.

38
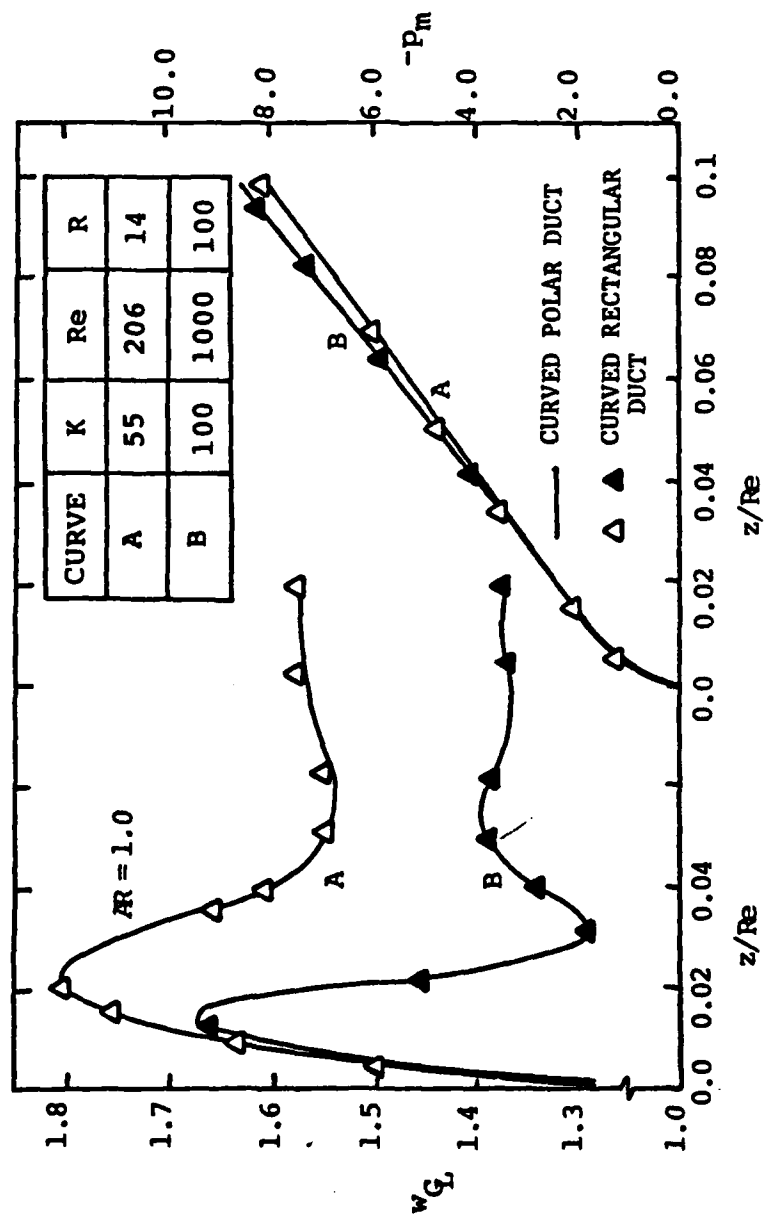
FIG. 4. STREAMWISE VARIATION OF CENTERLINE AXIAL VELOCITY AND MEAN VISCOUS PRESSURE FOR CURVED POLAR DUCTS.

$Re_w = -50$
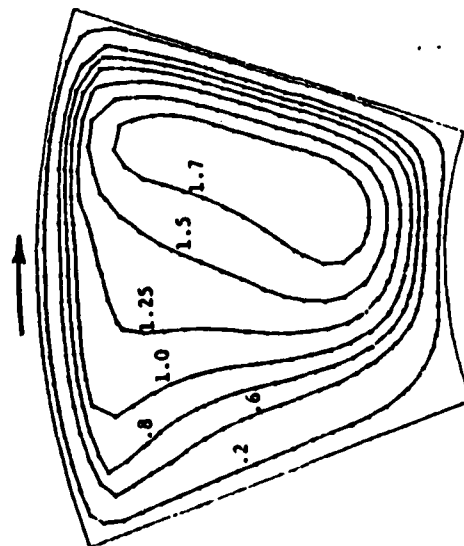
$Re_w = 0$
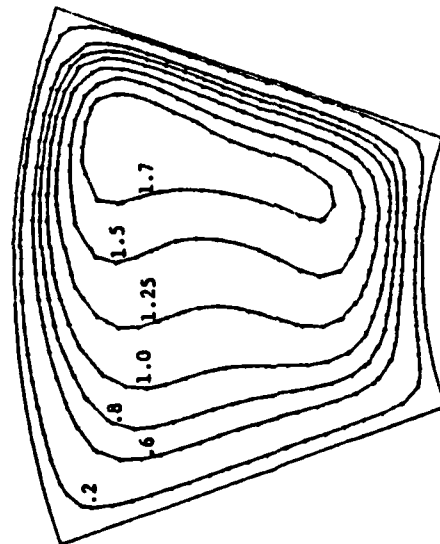
$Re_w = +50$
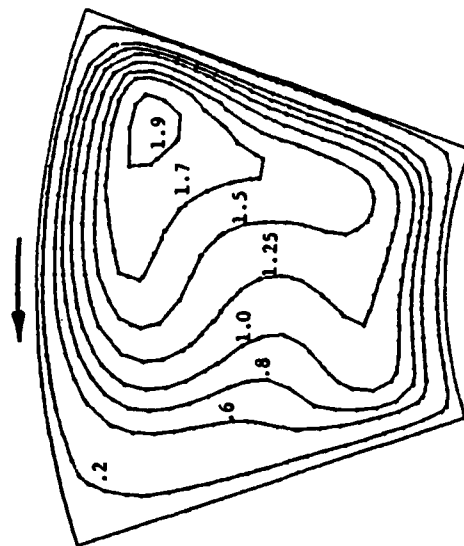
$Re = 1000, \quad R = 100, \quad K = 100, \quad AR = 1.0$

FIG. 5a. EFFECT OF WALL ROTATION ON FULLY DEVELOPED AXIAL VELOCITY CONTOURS.

$Re_w = -50$

$Re_w = 0$

$Re_w = +50$
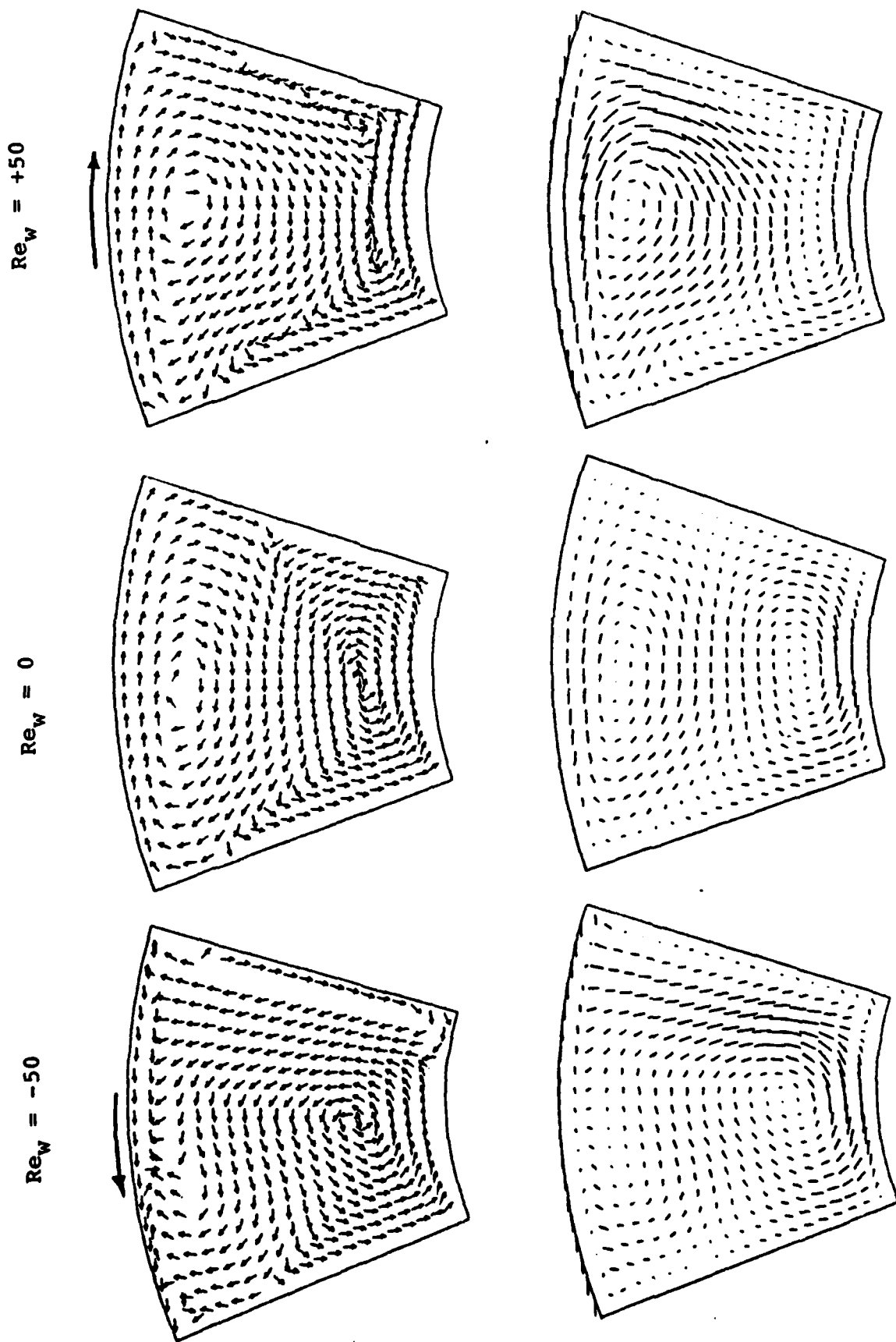
Re = 1000,   R = 100,   K = 100,   AR = 1.0

FIG. 5b.   EFFECT OF WALL ROTATION ON FULLY DEVELOPED CROSS-FLOW VELOCITY VECTORS.
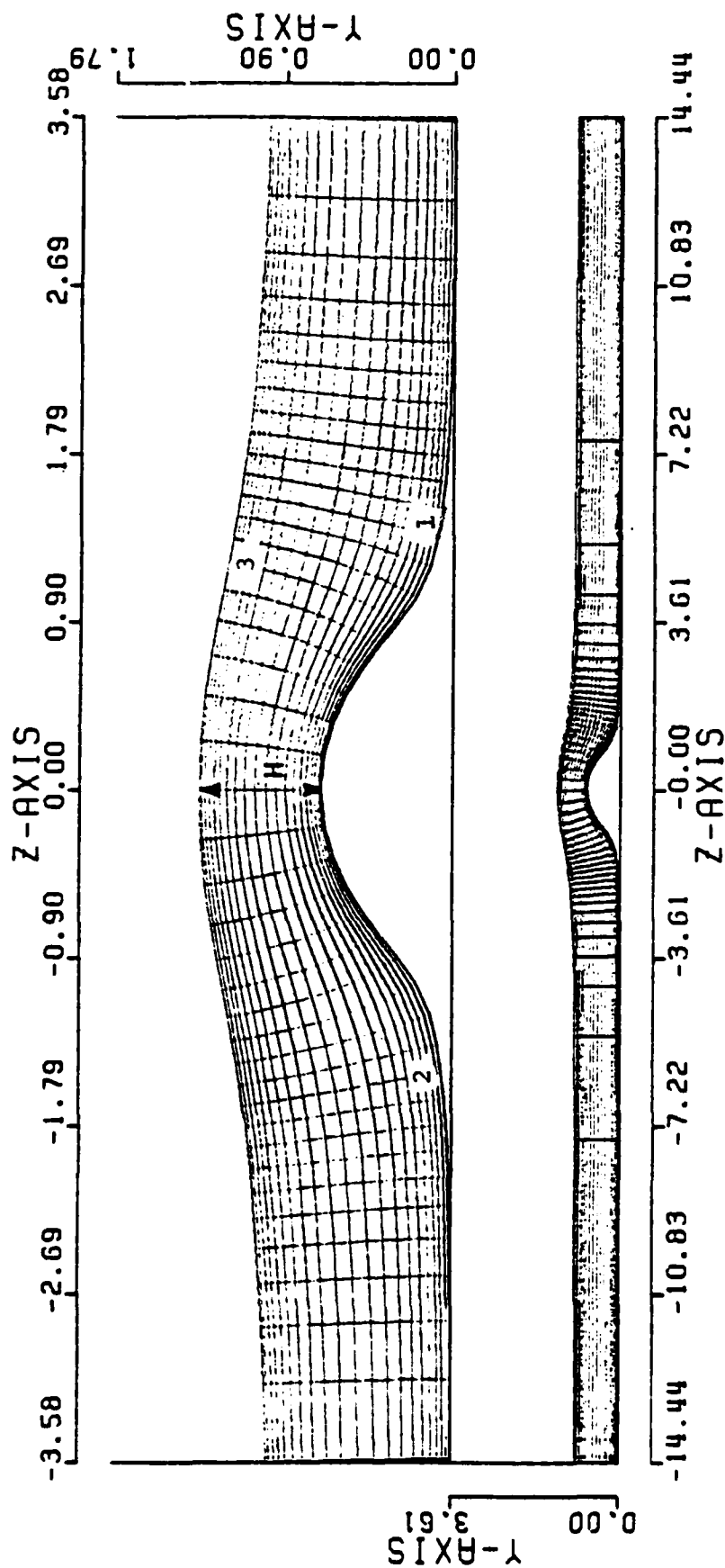
FIG. 6. TYPICAL CONFIGURATION AND COORDINATE DISTRIBUTION
FOR CHANNEL WITH ASYMETRIC CONSTRICTION.
A2 = 0.644, H = 0.643.
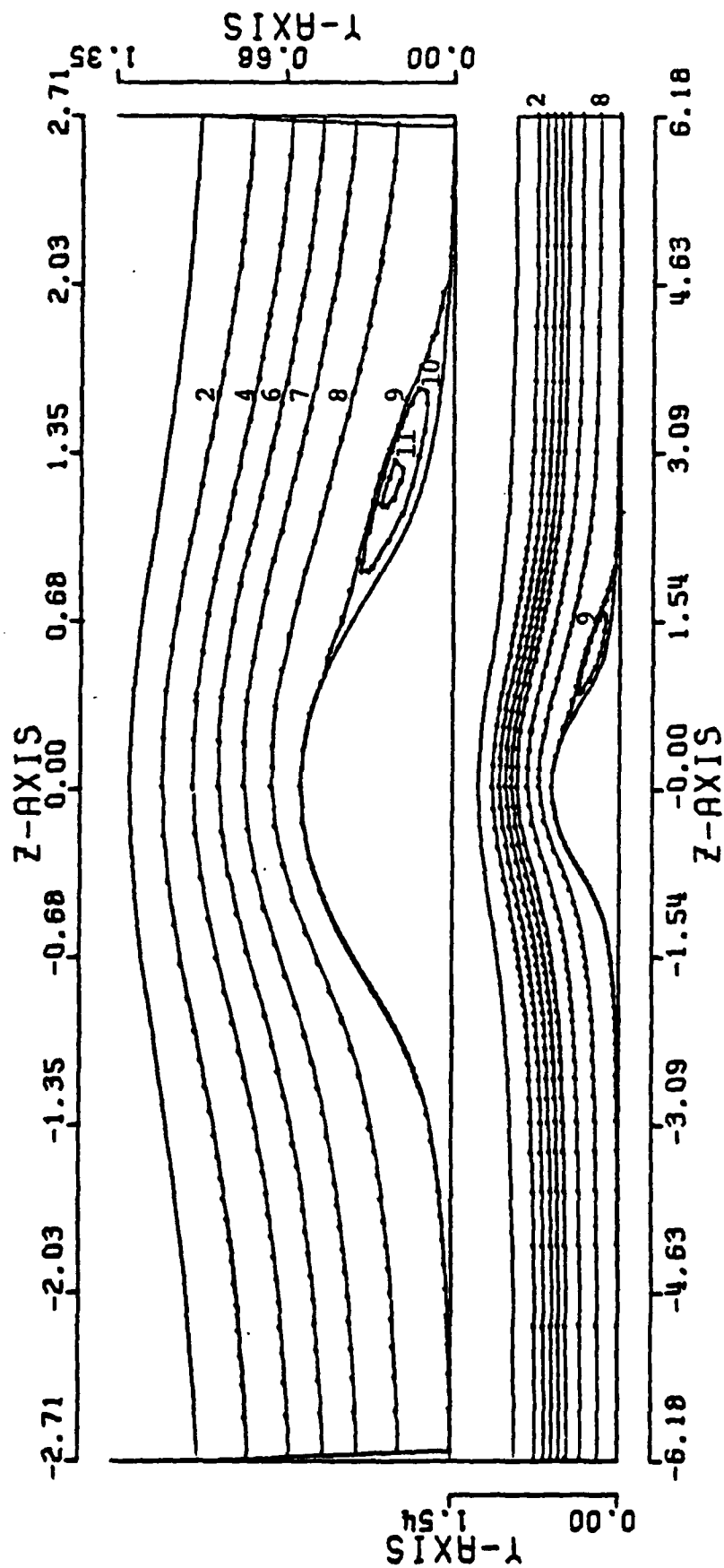
FIG. 7. STREAMLINE CONTOURS FOR CONSTRICTED CHANNEL

$R_E = 100$, $A2 = 0.585$, $H = 0.678$.

SEMI-ELLIPTIC SOLUTION

$c_{F,L} = \partial w/\partial n$ AT LOWER WALL

$c_{F,U} = \partial w/\partial n$ AT UPPER WALL

NAVIER-STOKES SOLUTION

$c_{F,L} = \partial w/\partial n$ AT LOWER WALL

$c_{F,U} = \partial w/\partial n$ AT UPPER WALL

$R_E = 100, \quad A2 = 0.585, \quad H = 0.678$

$c_{F,L}$

$c_{F,U}$

ZETA - AXIS

-6.27 -4.88 -3.48 -2.09 -0.70 0.70 2.09 3.48 4.88 6.27

SHEAR STRESS ALONG WALL

50.00 35.00 20.00 5.00 -10.00 -25.00 -40.00
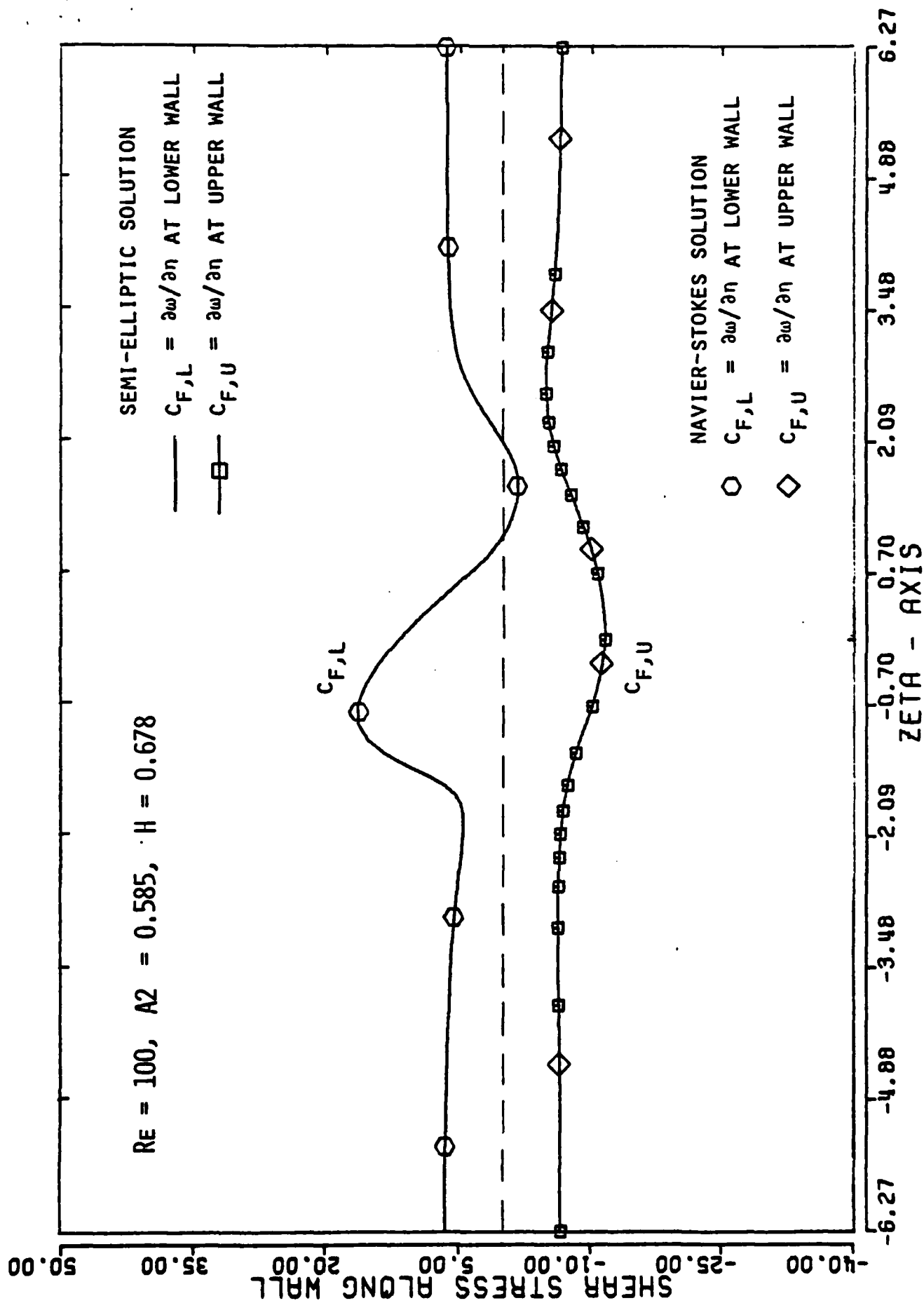
FIG. 8A. SHEAR-STRESS PARAMETER AT CHANNEL WALLS.
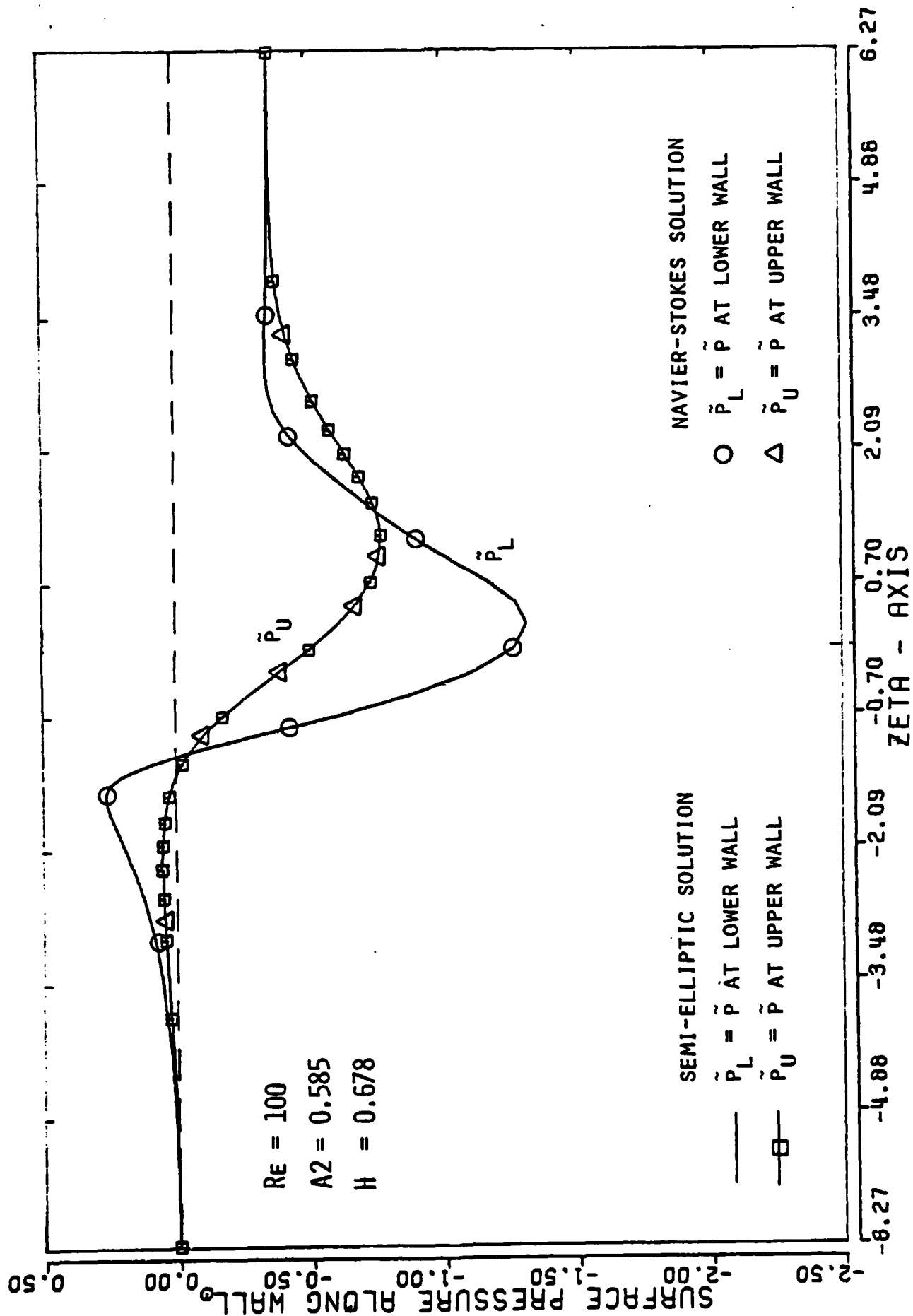
FIG. 8B. SURFACE-PRESSURE PARAMETER AT CHANNEL WALLS.

45
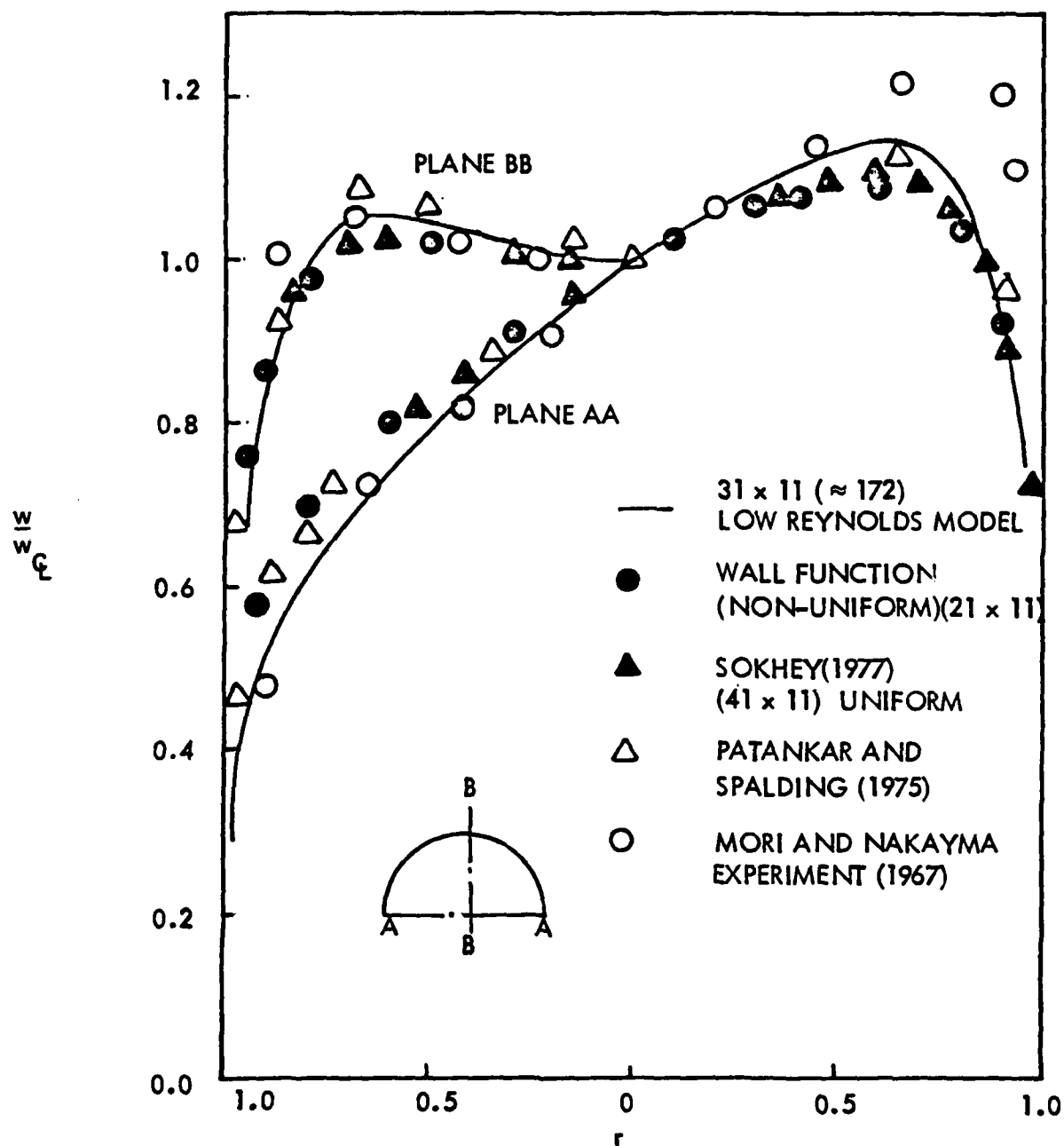
FIGURE 9. FULLY DEVELOPED AXIAL VELOCITY PROFILES IN CURVED CIRCULAR DUCT, $Re_D = 25000$, $R = 20$
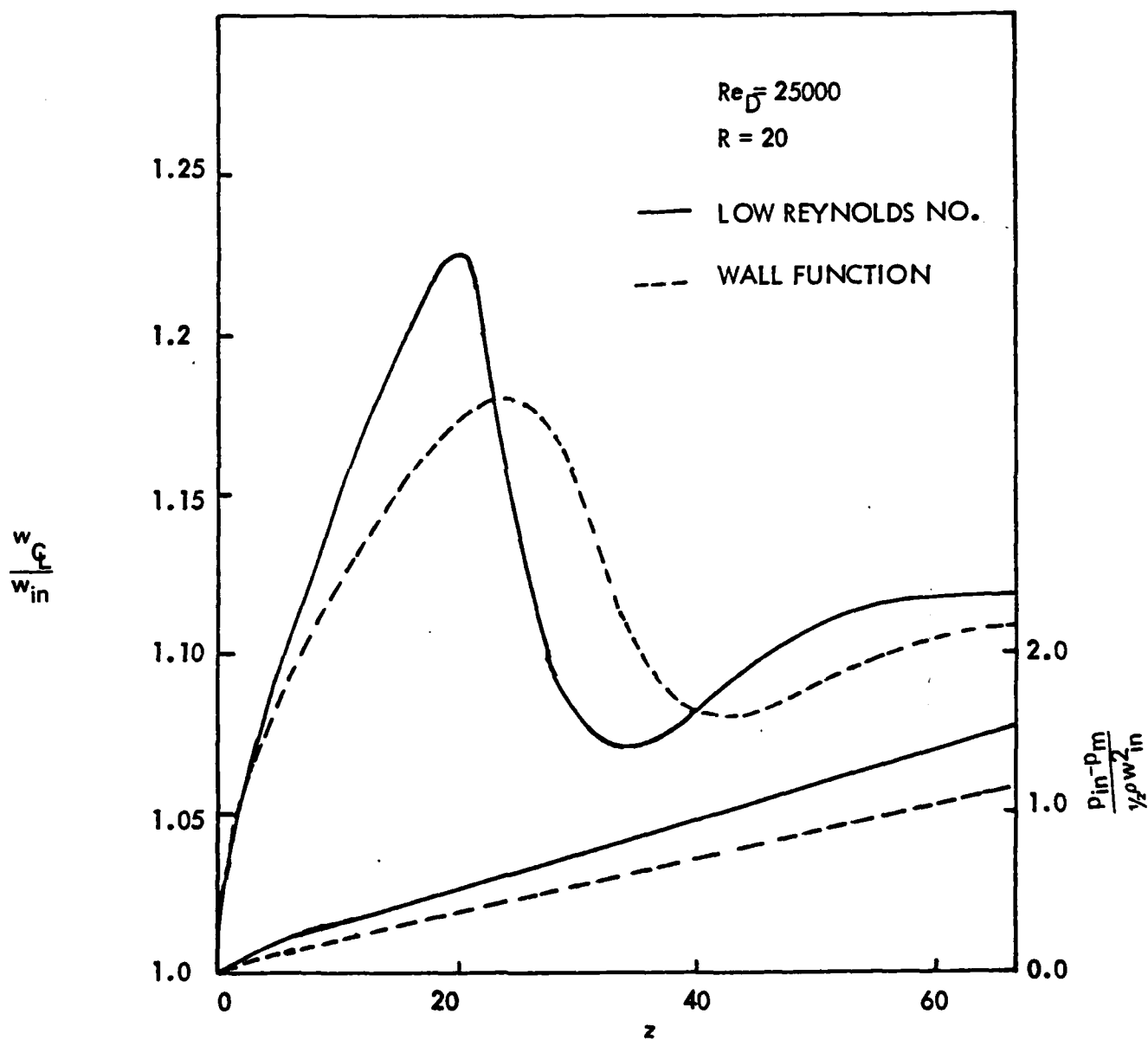
FIGURE 10. VARIATION OF AXIAL CENTER LINE VELOCITY AND
MEAN VISCOUS PRESSURE IN THE STREAM WISE
DIRECTION FOR A CURVED CIRCULAR PIPE
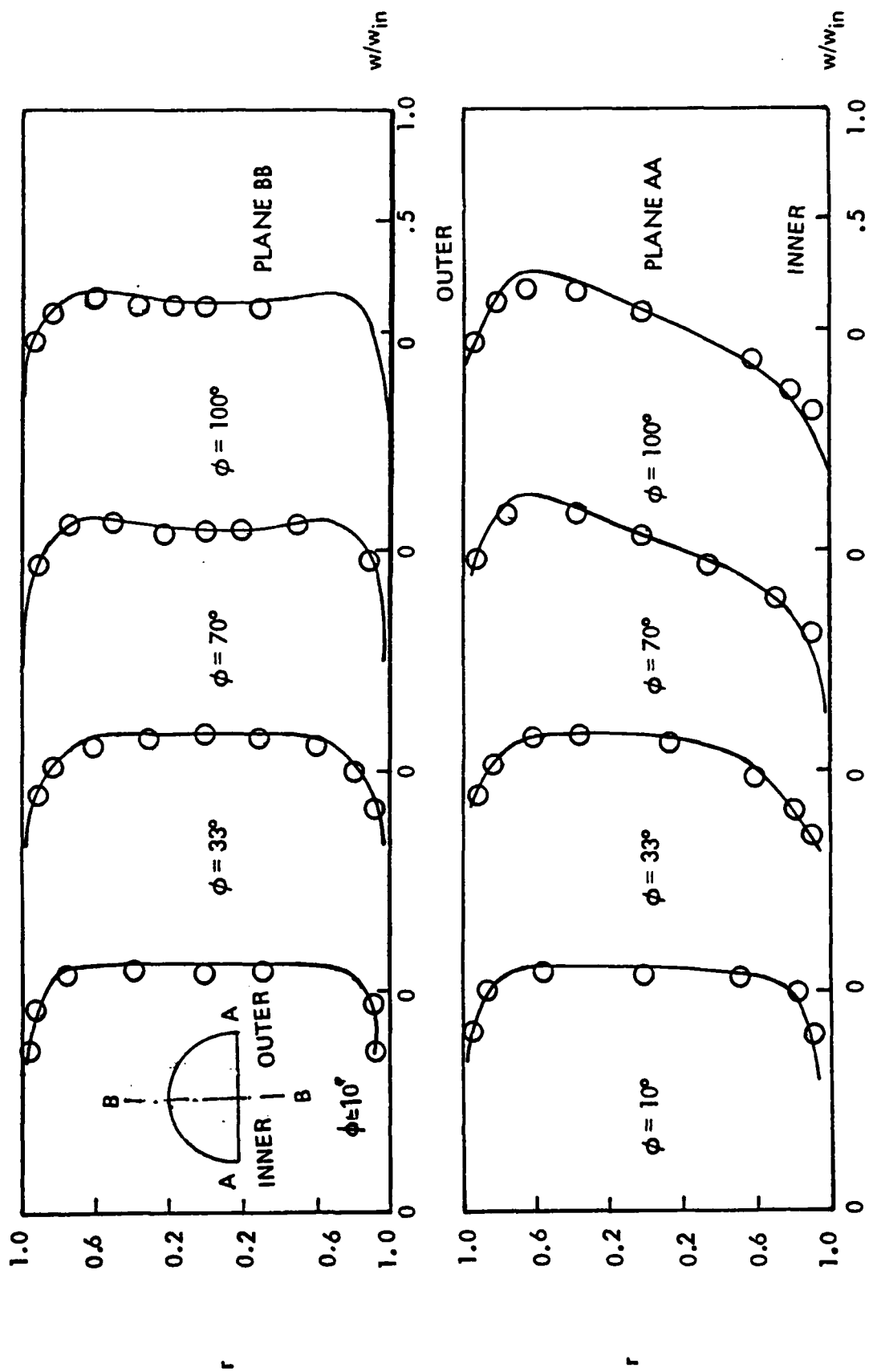
FIGURE 11.   DEVELOPMENT OF AXIAL VELOCITY PROFILES IN A CURVED CIRCULAR DUCT
(Re_D = 25000, R = 20); ———— LOW REYNOLDS MODEL; ○ WALL FUNCTION MODEL

48
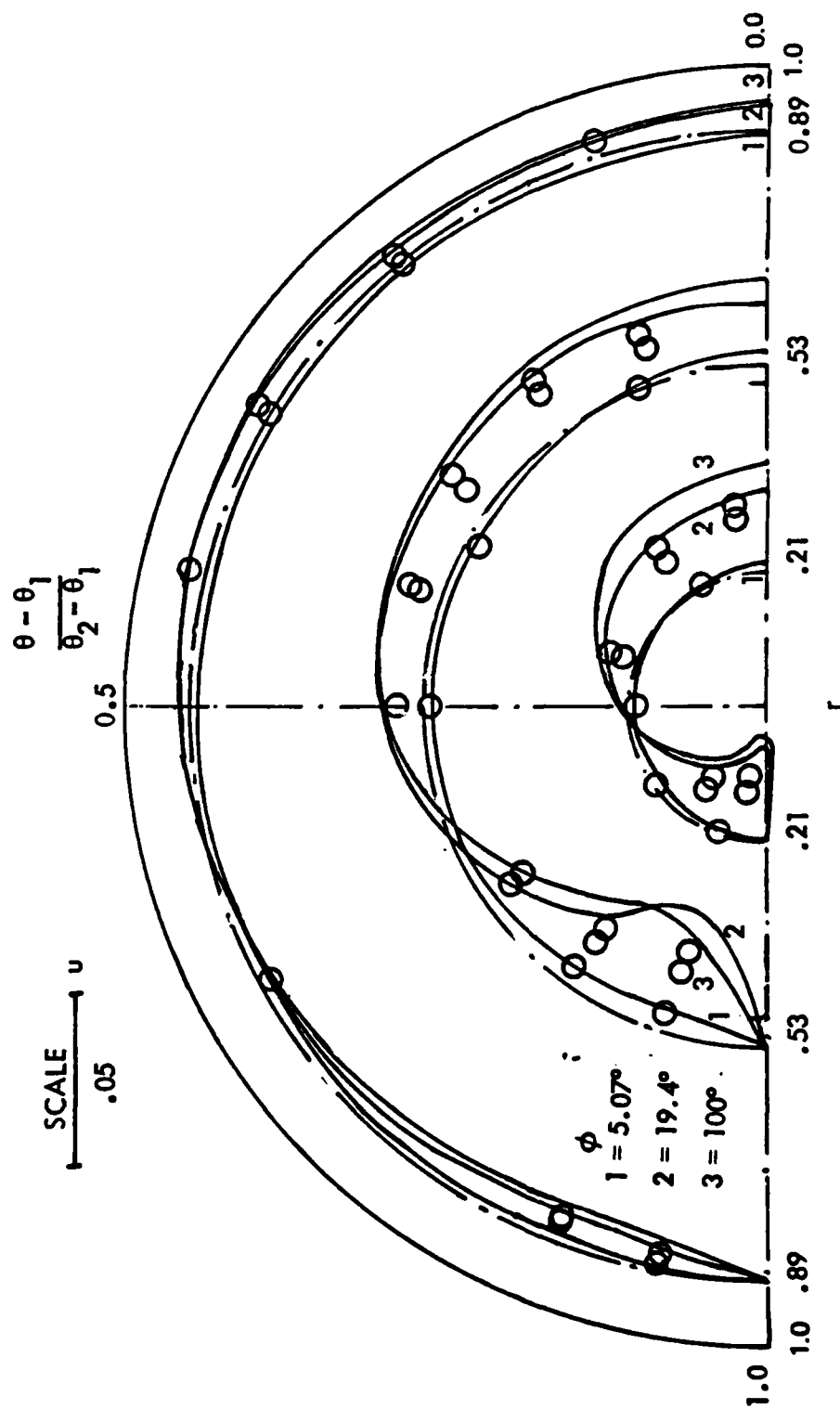
FIGURE 12a. DEVELOPING SECONDARY FLOW PROFILES IN A CURVED CIRCULAR DUCT, $Re_{\bar{D}}$ 2.5 × 10⁴, R = 20, — LOW REYNOLDS MODEL; O WALL FUNCTION MODEL
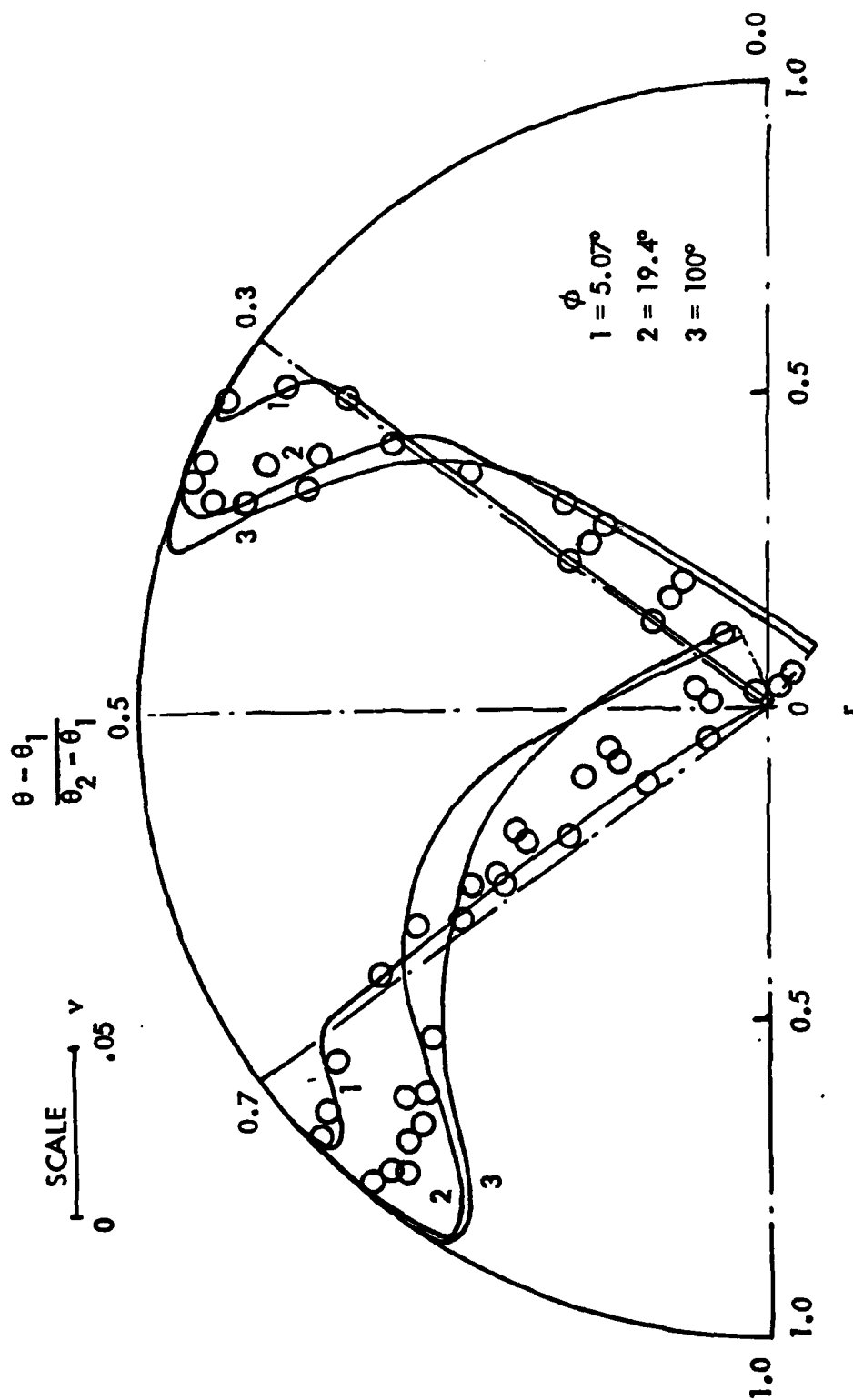
FIGURE 12b. DEVELOPMENT OF SECONDARY-FLOW VELOCITY PROFILES IN A CURVED CIRCULAR DUCT $Re_D \cong 2.5 \times 10^4$, $R = 20$; LOW REYNOLDS MODEL O WALL FUNCTION MODEL

$$\frac{\theta - \theta_1}{\theta_2 - \theta_1}$$

$$\varphi$$
$$1 = 5.07°$$
$$2 = 19.4°$$
$$3 = 100°$$

SCALE
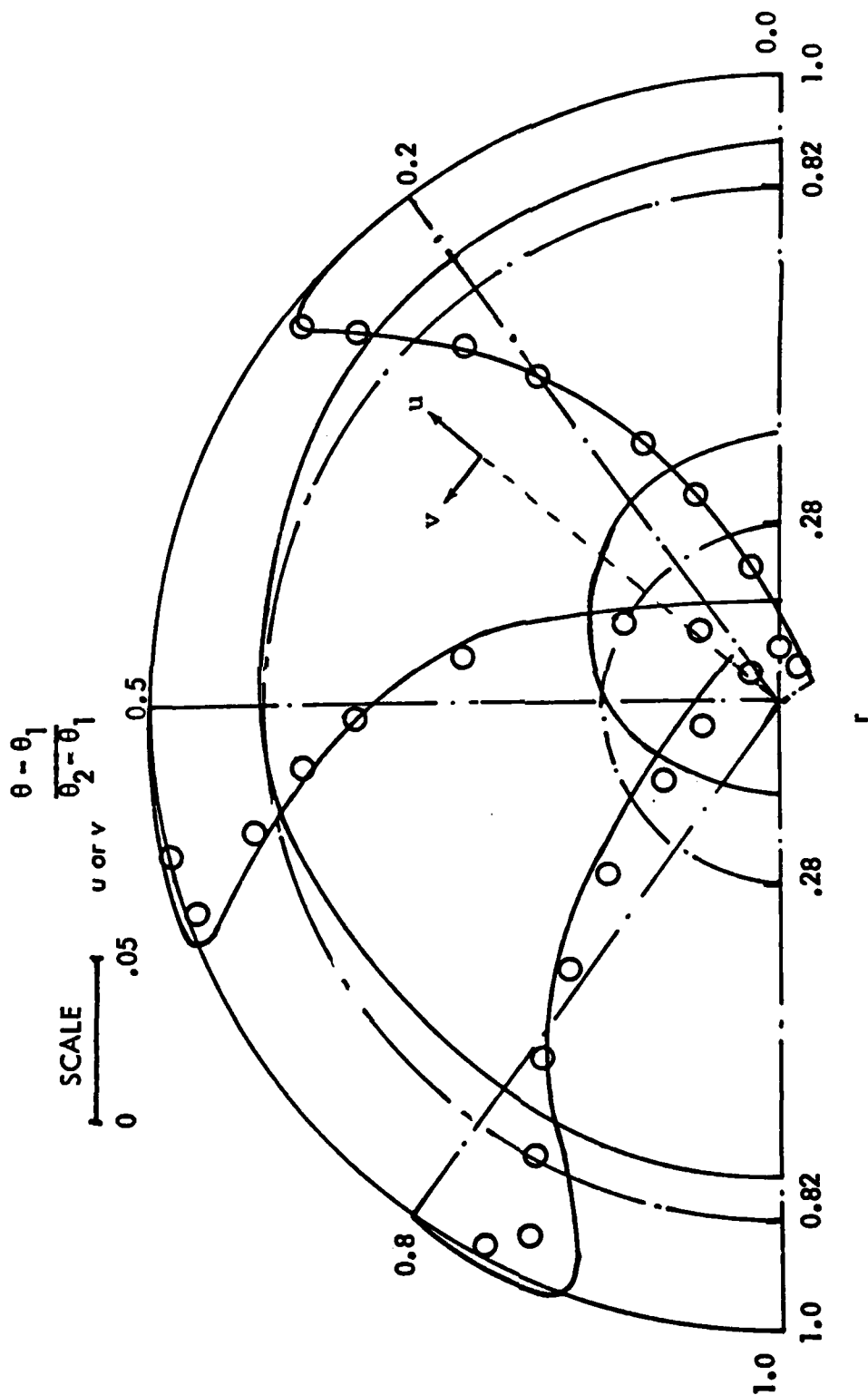
FIGURE 12c. FULLY DEVELOPED SECONDARY-FLOW VELOCITY PROFILES IN A CURVED CIRCULAR DUCT, $Re_D = 25000$, $R = 20$; — LOW REYNOLDS MODELLING; O WALL FUNCTION MODEL
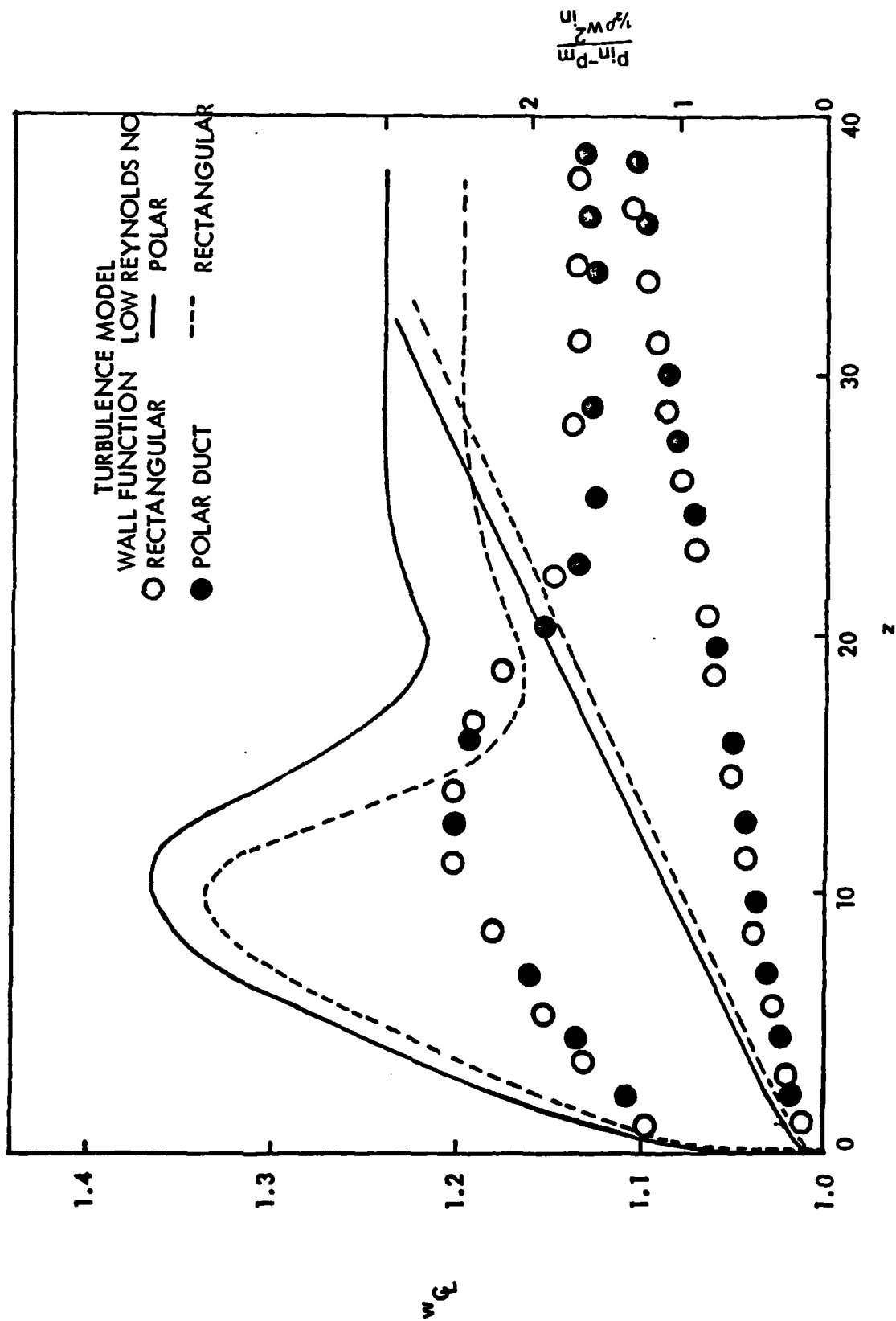
FIGURE 13. COMPARISON OF STREAM WISE VARIATION OF CENTER LINE AXIAL VELOCITY AND MEAN VISCOUS PRESSURE FOR CURVED POLAR AND CURVED SQUARE DUCTS, $Re_{\bar{D}} = 25000$, $R = 20$, $AR = 1$
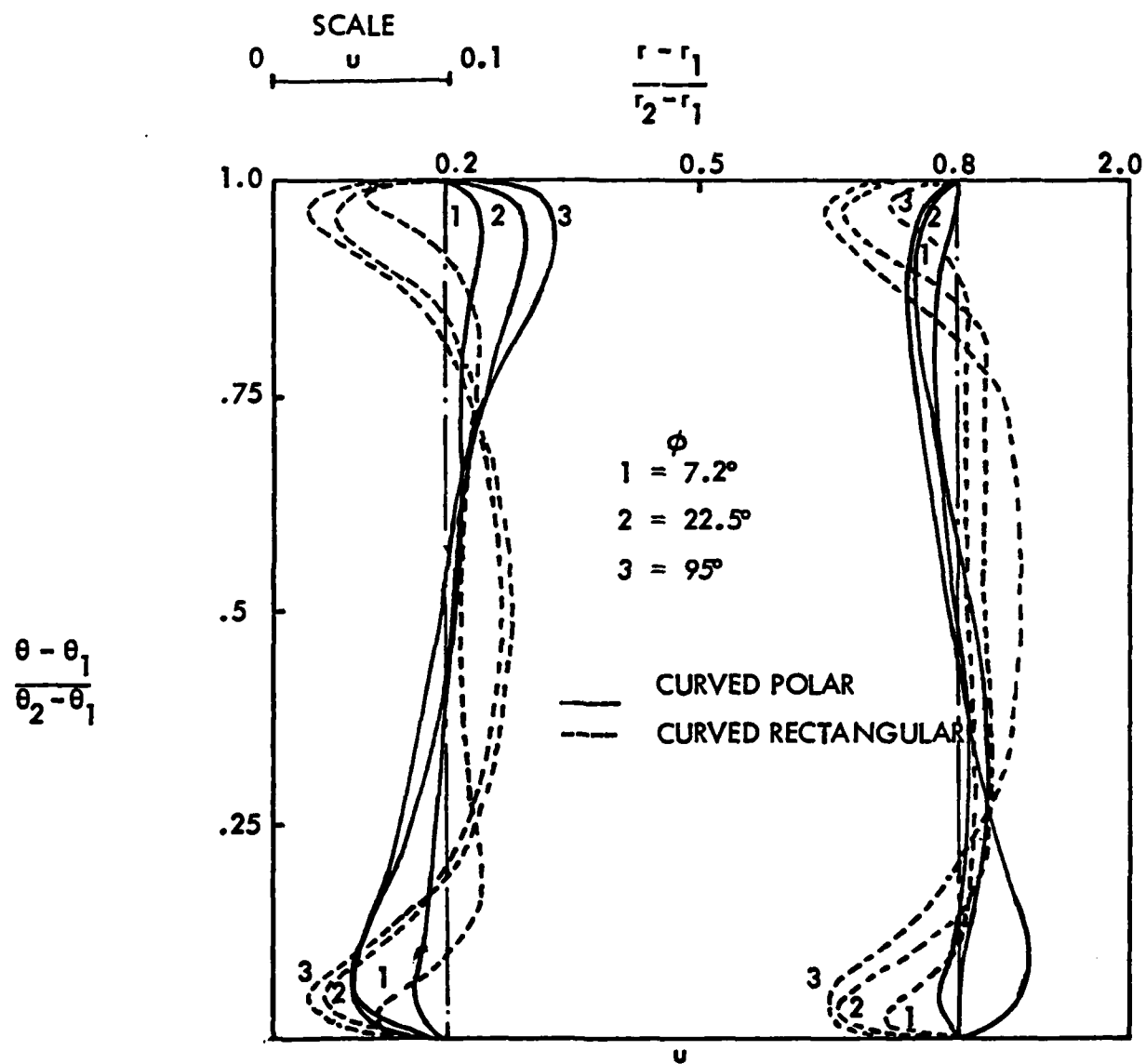
FIGURE 14a. DEVELOPING SECONDARY VELOCITY PROFILES FOR A
CURVED POLAR DUCT AND RECTANGULAR DUCT USING
LOW REYNOLDS MODELLING, $Re_D = 25000$, AR = 1, R = 20
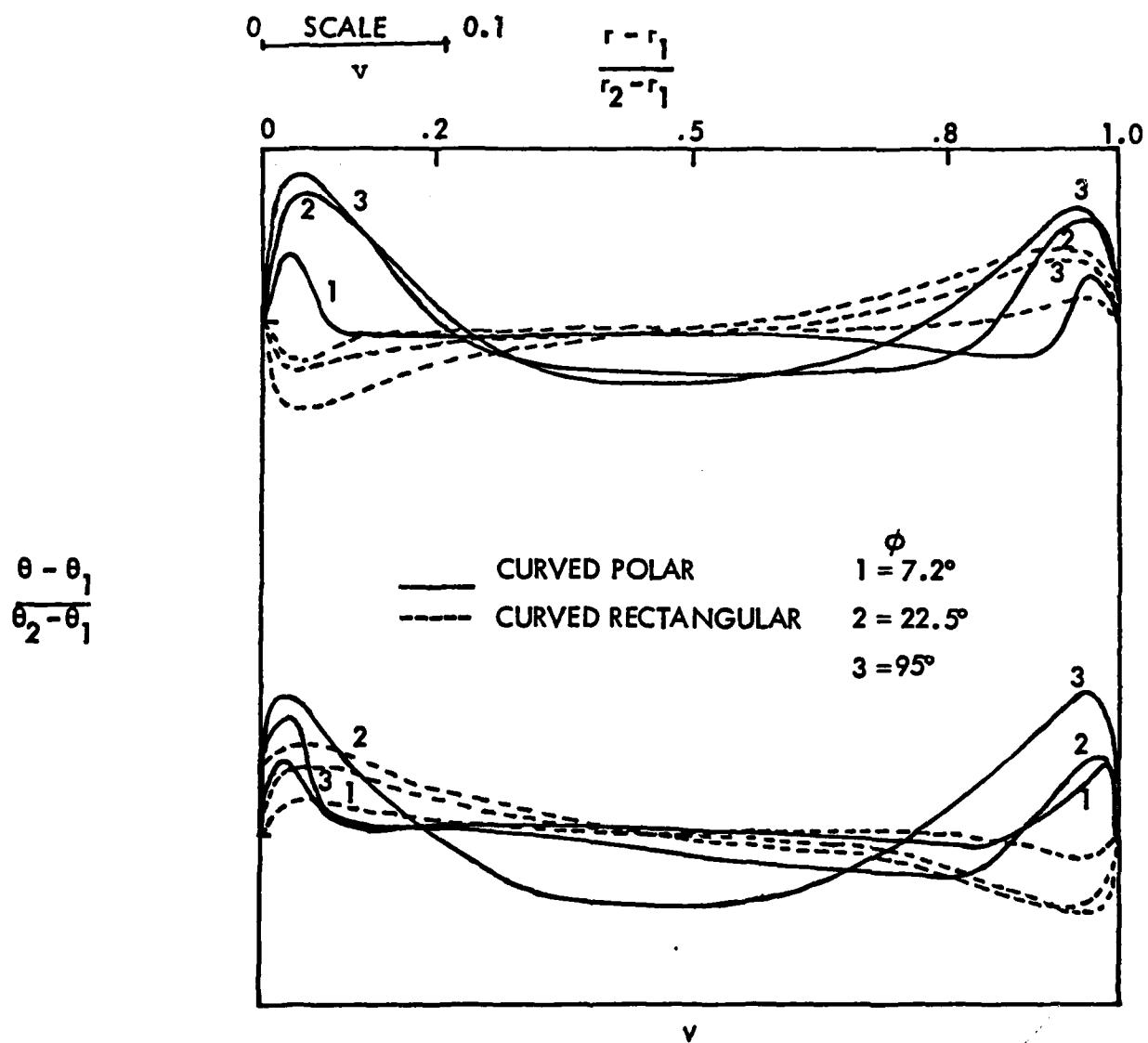
FIGURE 14b. DEVELOPING SECONDARY VELOCITY PROFILES FOR A
CURVED POLAR AND RECTANGULAR DUCT USING LOW
REYNOLDS TURBULENCE MODEL, $Re_D = 2.5 \times 10^4$, AR = 1,
R = 20
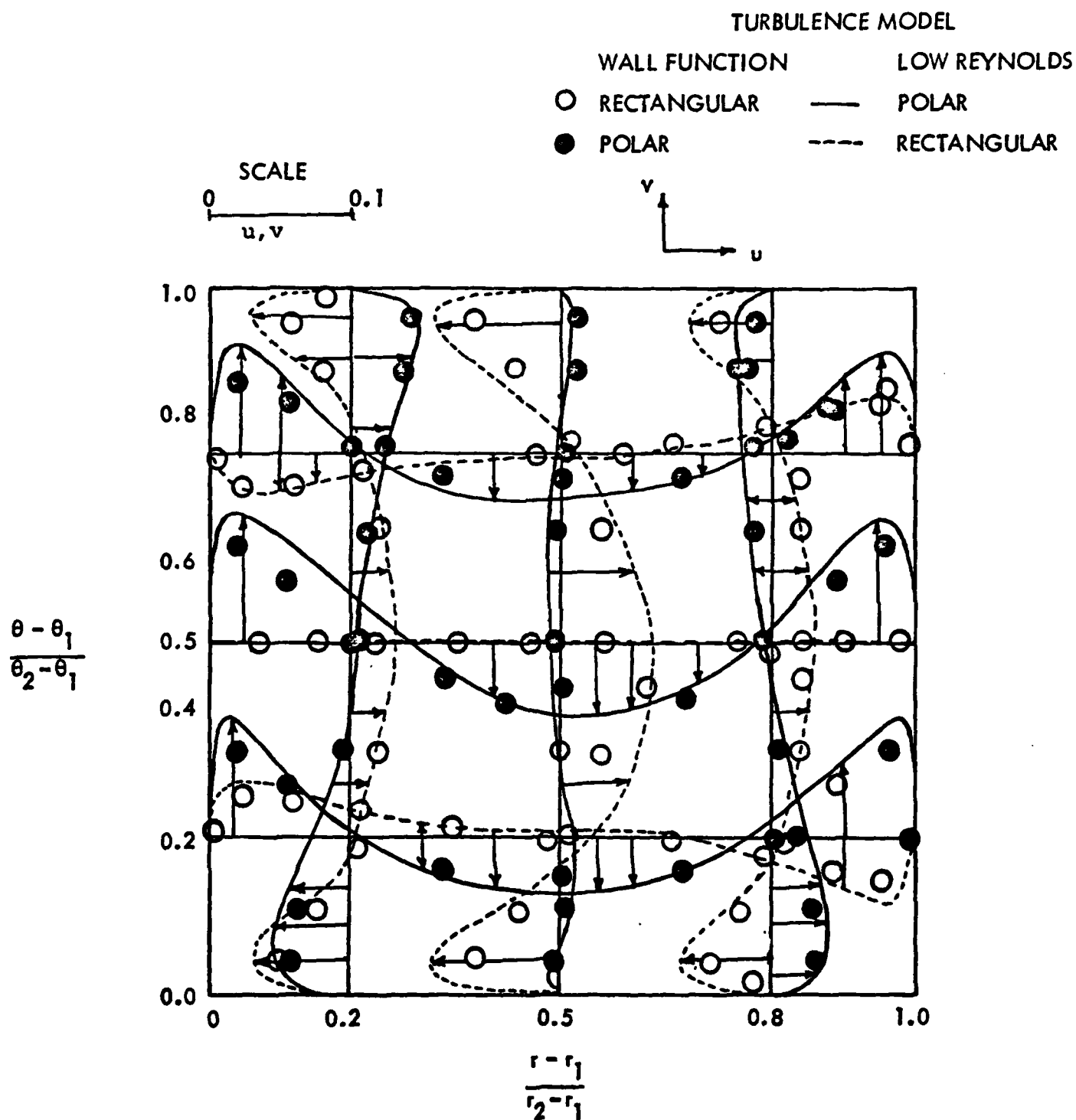
FIGURE 14c. FULLY DEVELOPED SECONDARY FLOW VELOCITY PROFILES IN A CURVED POLAR AND CURVED RECTANGULAR DUCT OF UNITY ASPECT RATIO, $Re_D = 25000$, $R = 20$
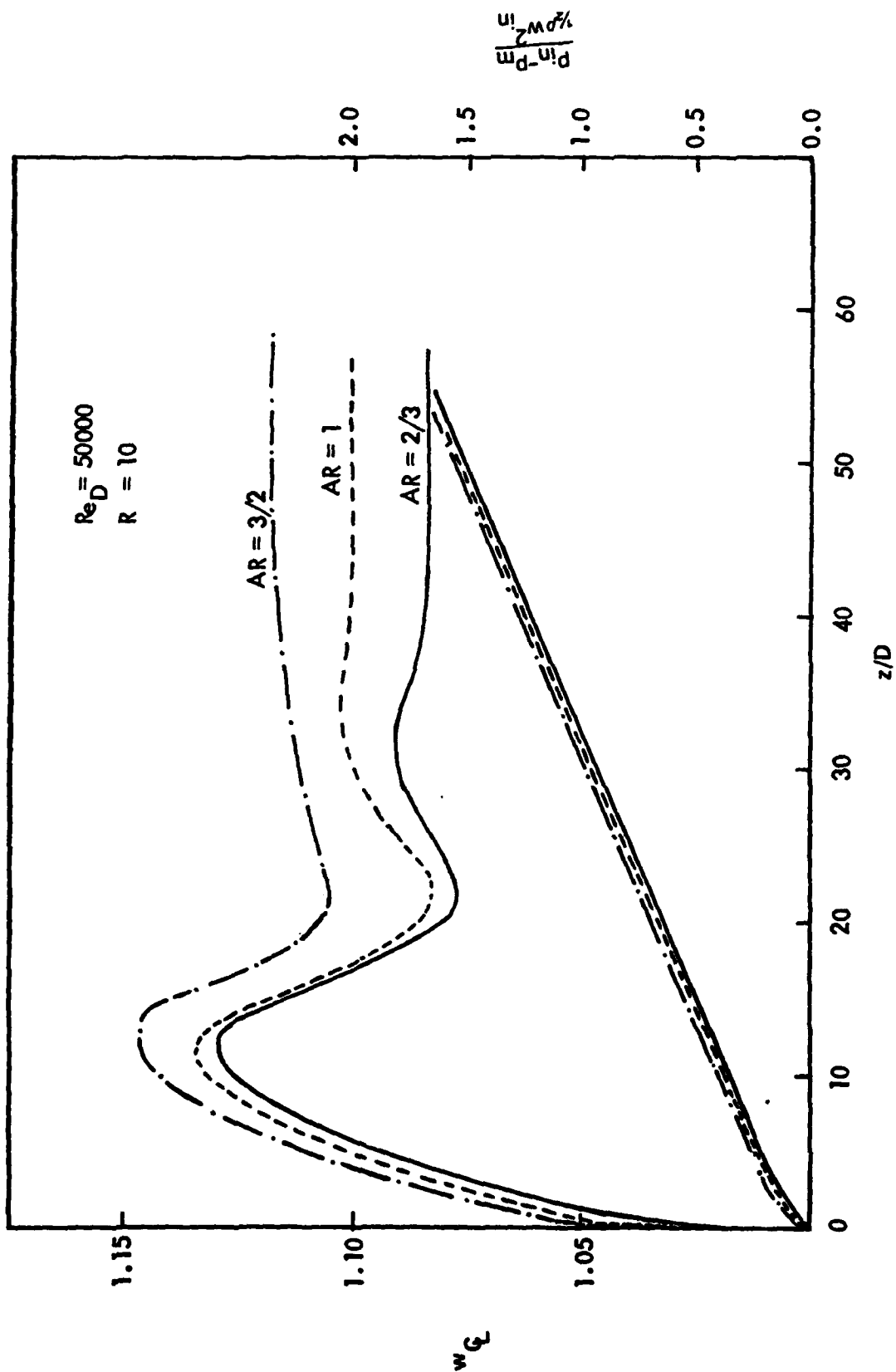
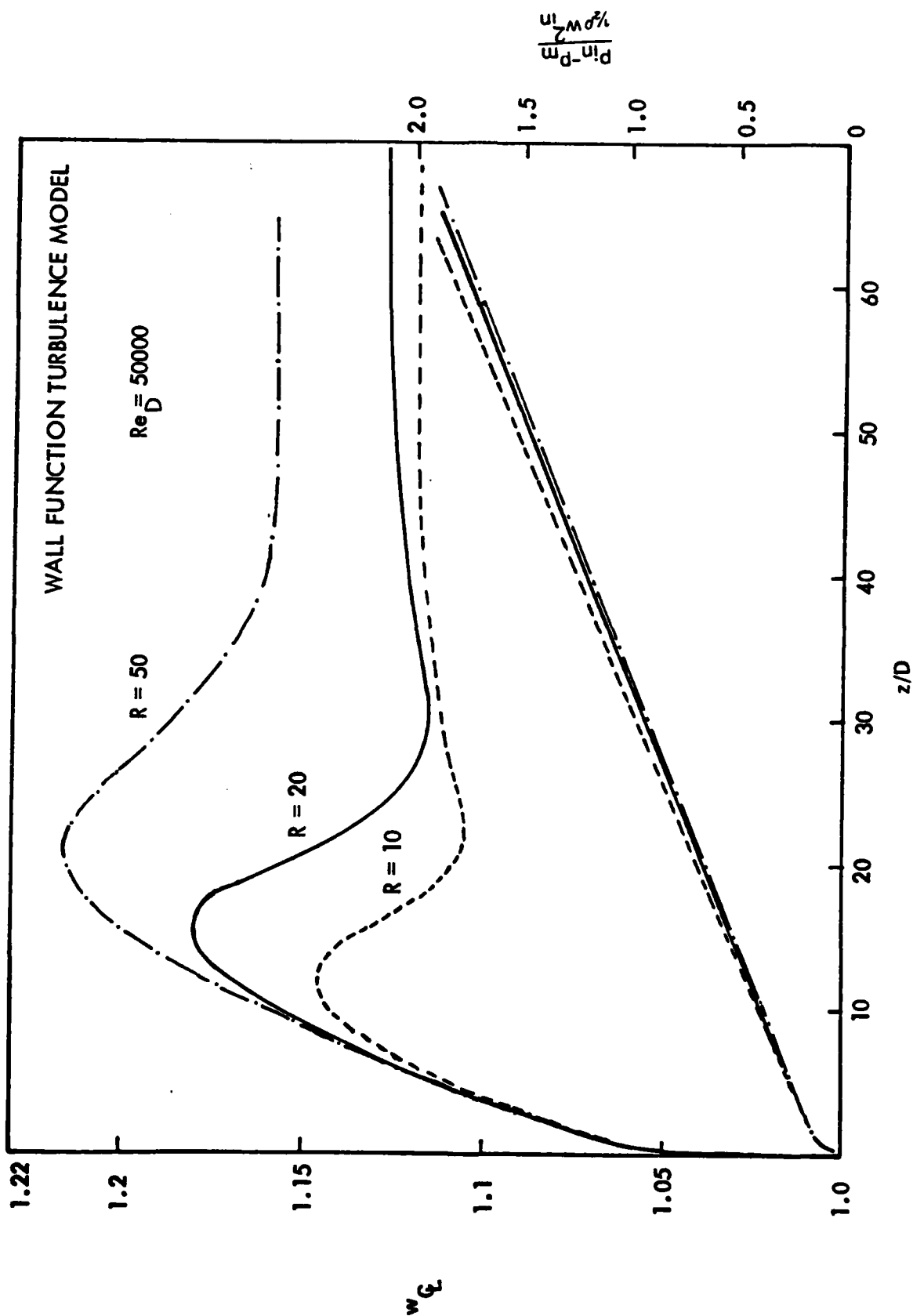**FIGURE 15. EFFECT OF ASPECT RATIO (AR) ON STREAM WISE CENTER LINE VELOCITY AND MEAN PRESSURE DROP IN A CURVED POLAR DUCT**

FIGURE 16. EFFECT OF CURVATURE RATIO ON THE STREAM WISE CENTER LINE VELOCITY $w_\mathbb{C}$ AND MEAN PRESSURE DROP IN A CURVED POLAR DUCT ($Re_D = 50000$; AR = 3/2)
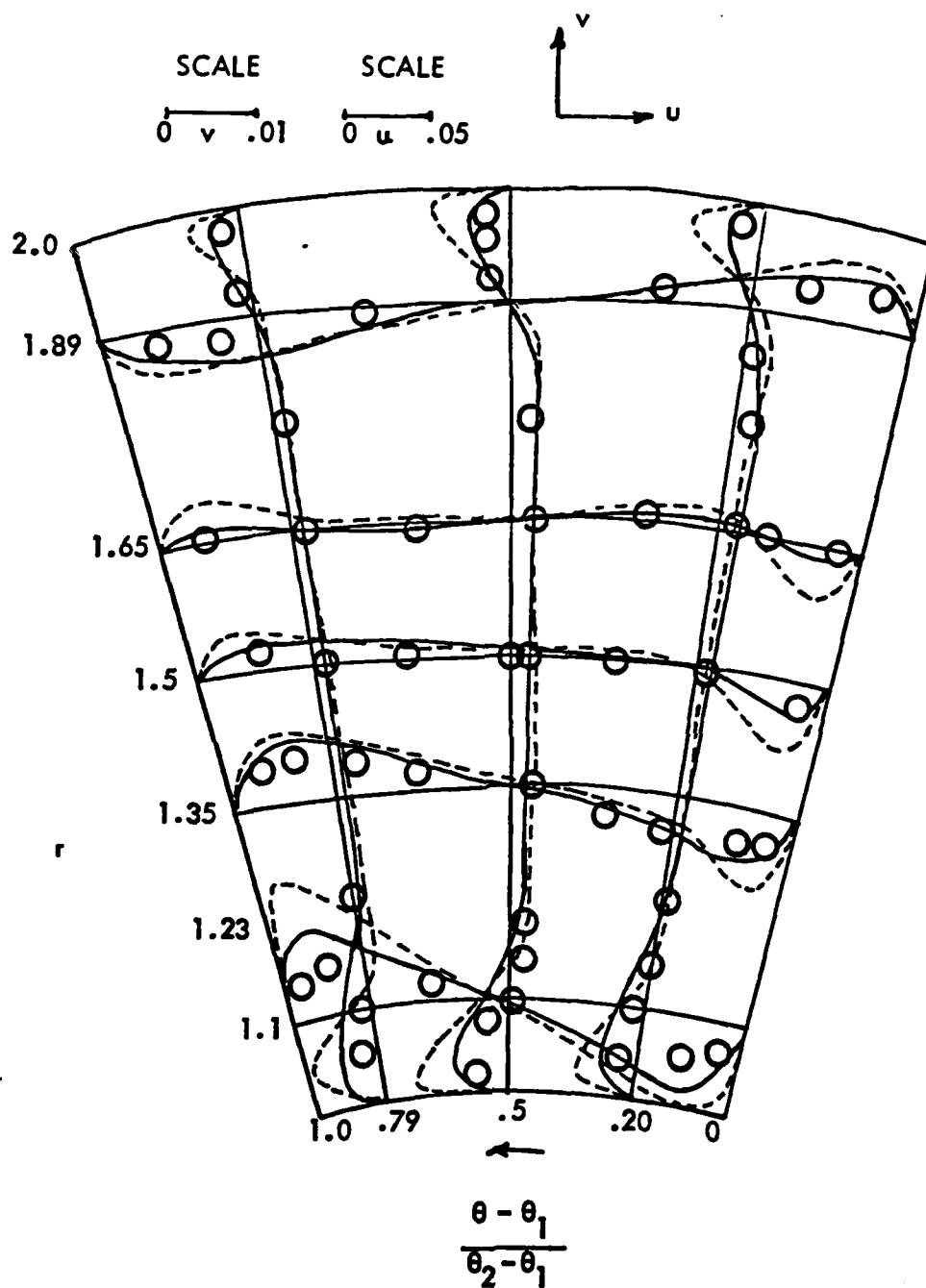
FIGURE 17. EFFECT OF CURVATURE RATIO ON FULLY DEVELOPED SECONDARY FLOW VELOCITY PROFILES FOR A CURVED POLAR DUCT
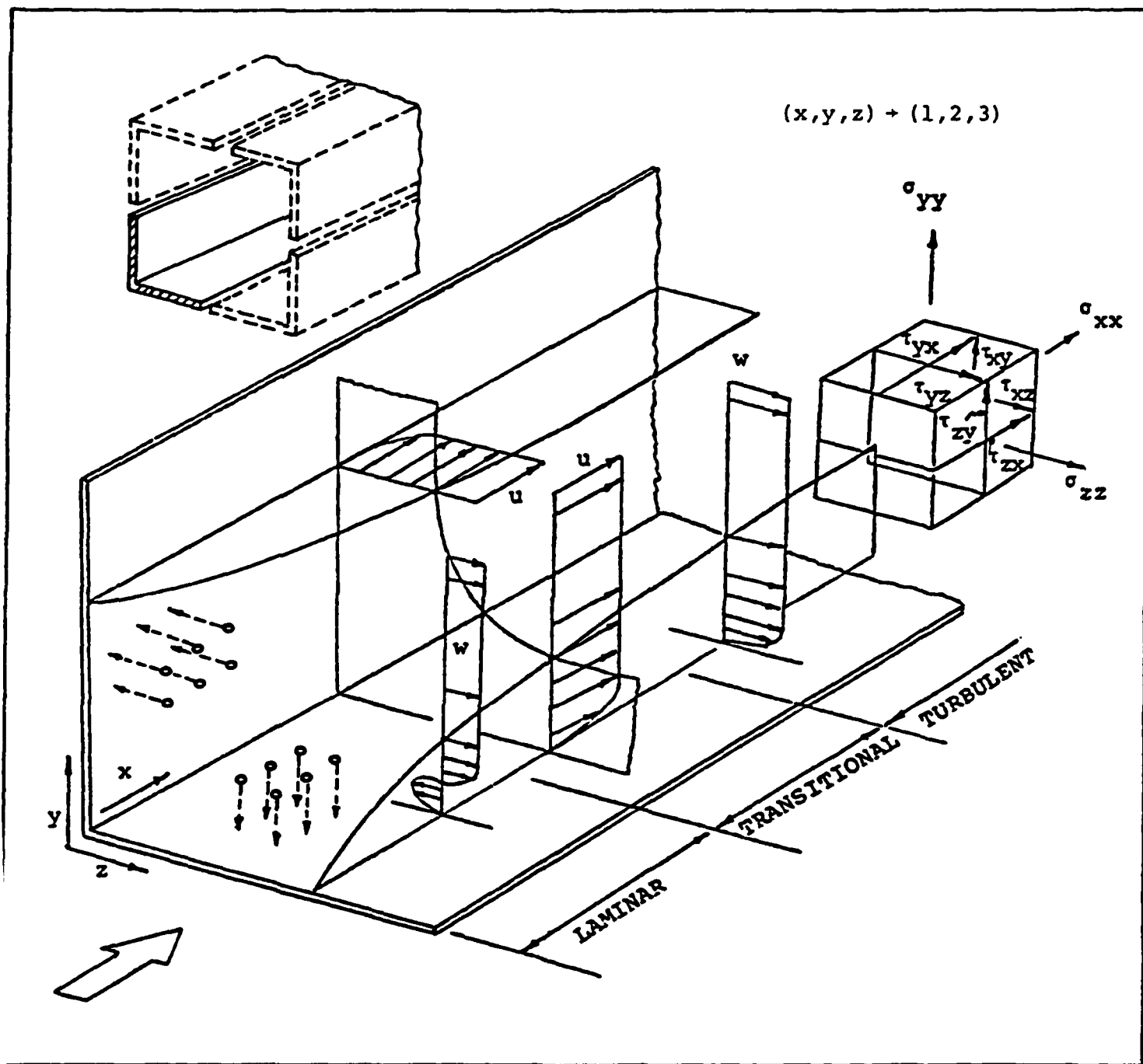Re_D = 50000, AR = 3/2, ---- R = 10, —— R = 20, O R = 50
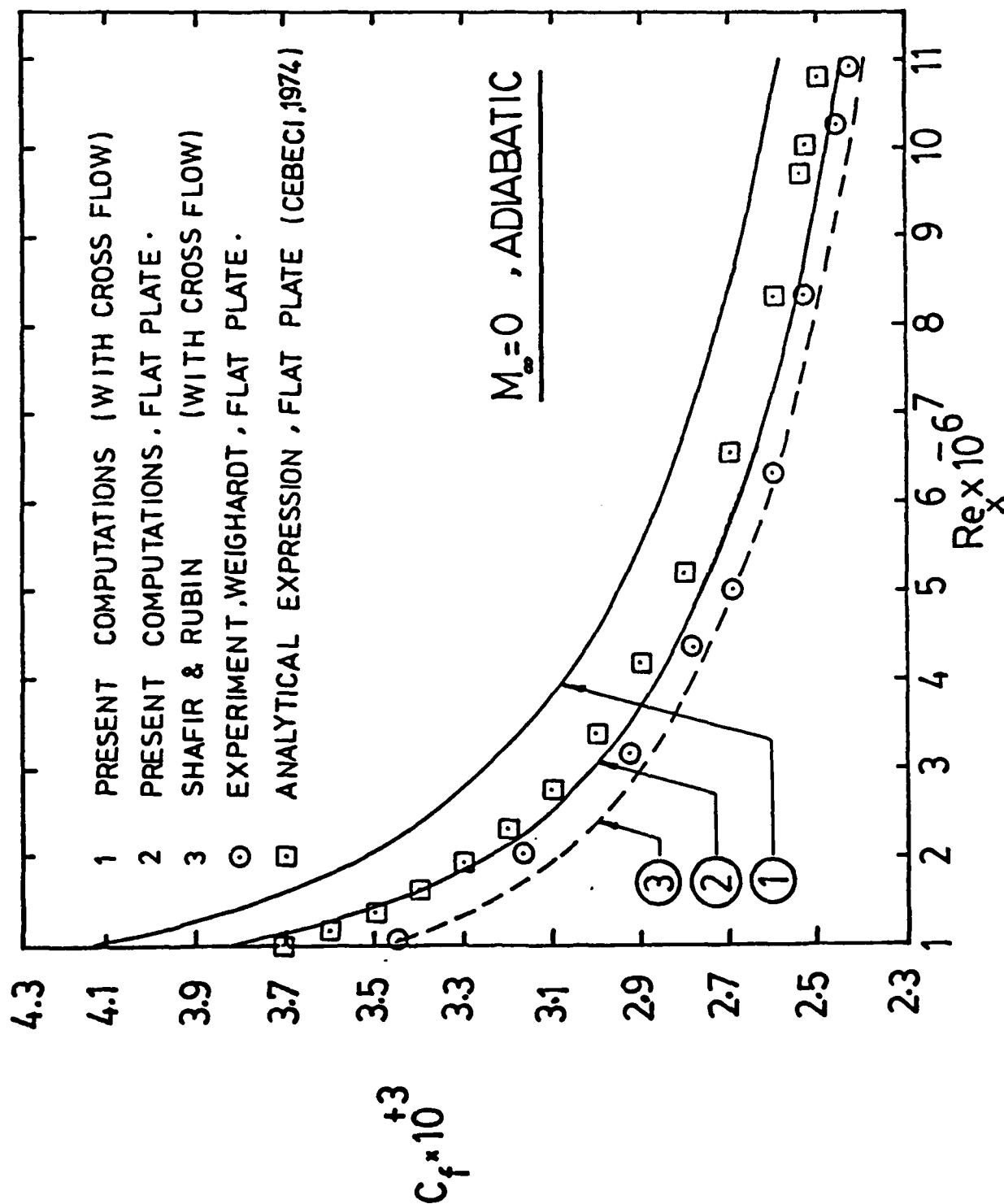
58

FIG. 18. CORNER-FLOW GEOMETRY AND NOMENCLATURE.

59

FIG. 19. COMPARATIVE STUDY OF STREAMWISE VARIATION IN SKIN-FRICTION COEFFICIENT.

The figure plots $C_f \times 10^{+3}$ (vertical axis, ranging from 2.3 to 4.3) against $Re_x \times 10^{-6}$ (horizontal axis, ranging from 1 to 11) for the condition $M_\infty = 0$, ADIABATIC.

Legend:
1 — PRESENT COMPUTATIONS (WITH CROSS FLOW)
2 — PRESENT COMPUTATIONS, FLAT PLATE.
3 — SHAFIR & RUBIN (WITH CROSS FLOW)
$\odot$ — EXPERIMENT, WEIGHARDT, FLAT PLATE.
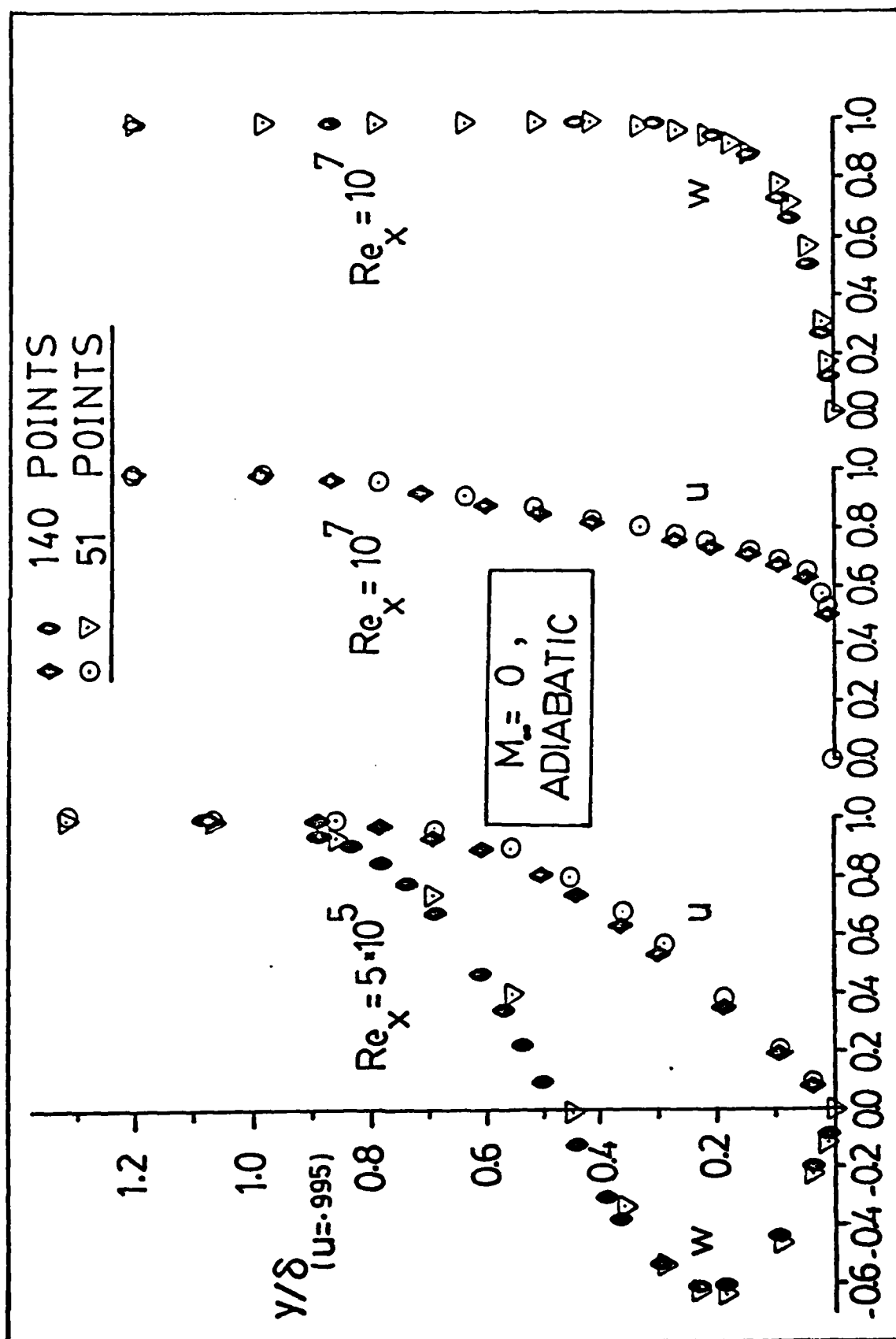$\boxdot$ — ANALYTICAL EXPRESSION, FLAT PLATE (CEBECI, 1974)

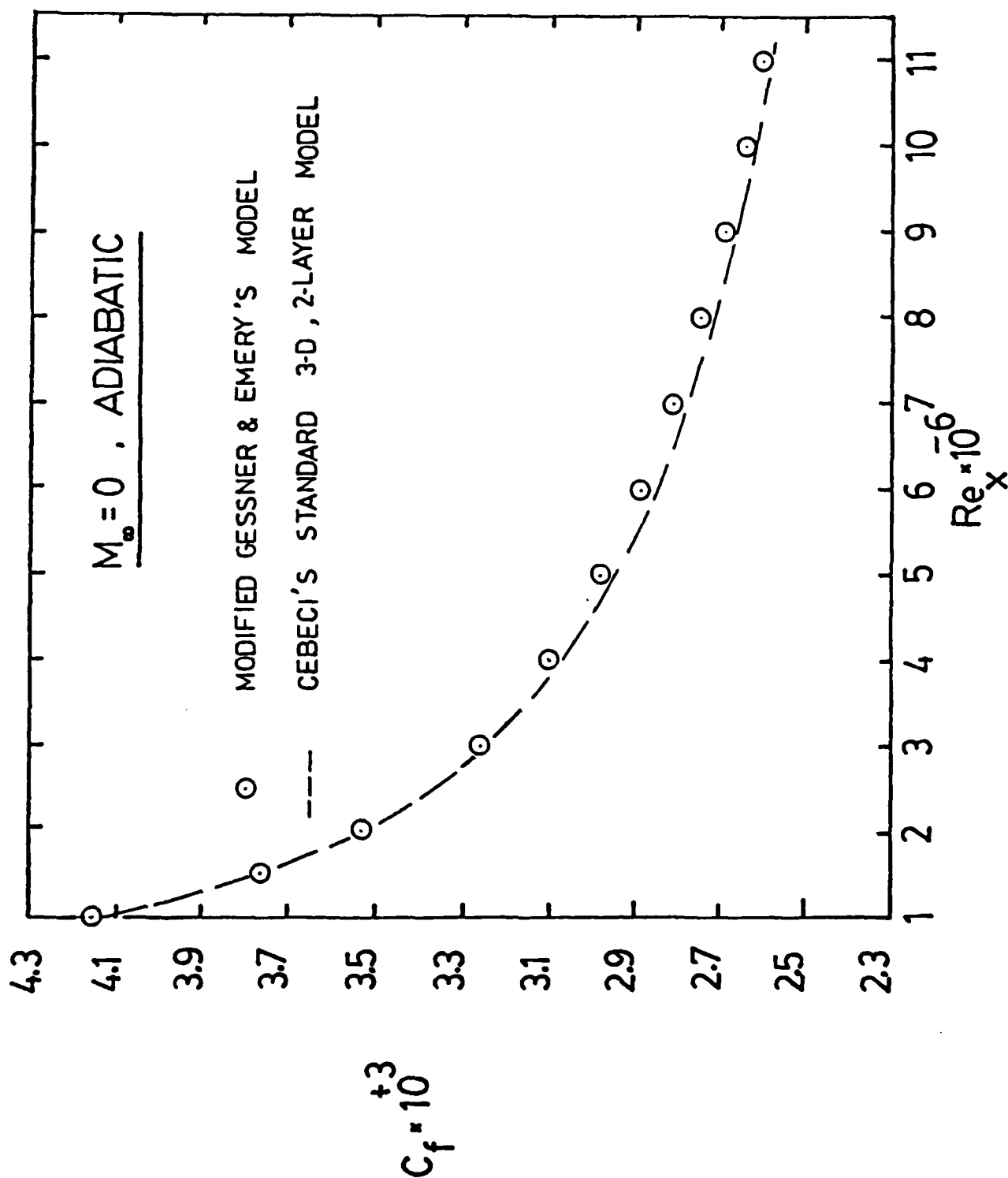FIG. 20. EFFECT OF NORMAL STEP SIZE ON VELOCITIES.
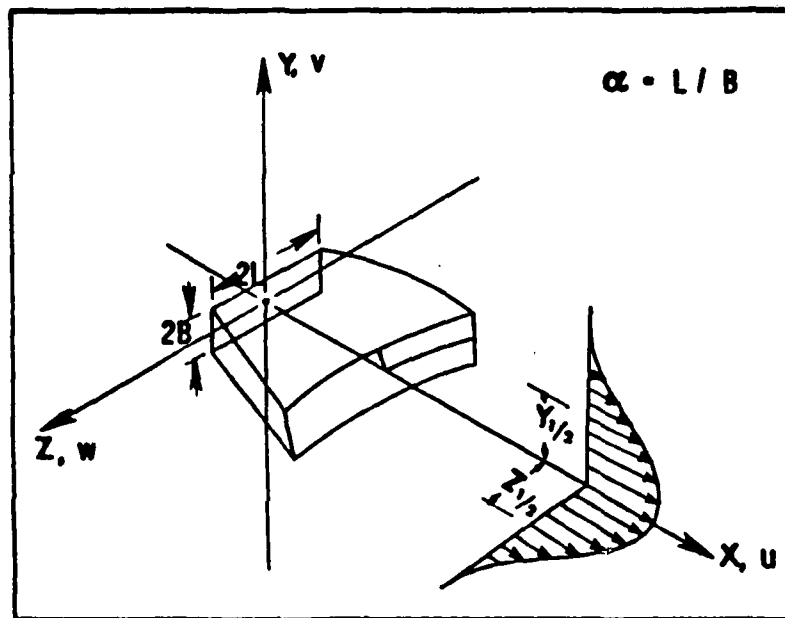
61

FIG. 21. COMPARATIVE STUDY OF ISOTROPIC AND ANISOTROPIC TURBULENCE MODELS.

FIG. 22. SCHEMATIC OF JET FLOW CONFIGURATION.